

Compositional Generalization Requires More Than Disentangled Representations

Qiyao Liang^{*1} Daoyuan Qian^{*2} Liu Ziyin¹³ Ila Fiete¹

Abstract

Composition—the ability to generate myriad variations from finite means—is believed to underlie powerful generalization. However, compositional generalization remains a key challenge for deep learning. A widely held assumption is that learning *disentangled* (factorized) representations naturally supports this kind of extrapolation. Yet, empirical results are mixed, with many generative models failing to recognize and compose factors to generate out-of-distribution (OOD) samples. In this work, we investigate a controlled 2D Gaussian “bump” generation task, demonstrating that standard generative architectures fail in OOD regions when training with partial data, even when supplied with fully disentangled (x, y) coordinates, re-entangling them through subsequent layers. By examining the model’s learned kernels and manifold geometry, we show that this failure reflects a “memorization” strategy for generation through the superposition of training data rather than by combining the true factorized features. We show that models forced—through architectural modifications with regularization or curated training data—to create disentangled representations in the full-dimensional representational (pixel) space can be highly data-efficient and effective at learning to compose in OOD regions. These findings underscore that bottlenecks with factorized/disentangled representations in an abstract representation are insufficient: the model must actively maintain or induce factorization directly in the representational space in order to achieve robust compositional generalization.

^{*}Equal contribution ¹Massachusetts Institute of Technology, Cambridge MA, USA 02139 ²University of Cambridge, Cambridge CB2 1EW, U.K ³NTT Research. Correspondence to: Qiyao Liang <qiyao@mit.edu>.

1. Introduction

A core motivation for disentangled representation learning is the belief that factoring an environment into independent latent dimensions, or “concepts”, should lead to powerful combinatorial generalization: if a model can learn the representation of each factor separately, then in principle it can synthesize new combinations of those factors without extensive retraining. This property is often referred to as *compositional generalization* and is considered crucial for data efficiency and robust extrapolation in high-dimensional tasks, such as language understanding and vision (Lake & Baroni, 2018).

Despite many attempts, disentangled representation learning has shown mixed results when it comes to compositional generalization. Some studies report clear data-efficiency gains and OOD benefits (Higgins et al., 2017a; Chen et al., 2018), while others find no significant advantage or even detrimental effects (Locatello et al., 2019; Ganin et al., 2017). This tension motivates a deeper theoretical exploration:

Is a disentangled/factorized¹ representation alone sufficient for compositional generalization? If not, why, and what other ingredients or constraints are necessary?

In this paper, we develop a mechanistic perspective on why simply factorizing an intermediate (or input) representation often falls short of enabling robust out-of-distribution (OOD) generalization. Concretely, we focus on a synthetic 2D Gaussian “bump” generation task, where a network learns to decode (x, y) into a spatial image. We provide a detailed empirical investigation into why *disentangled representations* often fail to achieve robust compositional generalization. Specifically:

- From a manifold-based viewpoint, we show that while the input or bottleneck layer may be factorized, subsequent layers can “warp” and remix factors, leading to poor out-of-distribution (OOD) extrapolation.
- Using a kernel-based perspective, we show that networks

¹We use the terms “disentanglement” and “factorization” interchangeably. See Section A.2 for a discussion of the definitions and distinctions.

failing to compose have overwritten their factorized inputs by “memorizing” training data, rather than combining independent factors, and simply superpose memorized states when attempting OOD generalization.

- We use a Jacobian-based metric tensor to study the representational manifold, demonstrating how factorization erodes layer-by-layer in standard CNN decoders.
- Finally, we show that enforcing factorization directly in the output (pixel) space—through architectural constraints or curated datasets—enables the model to overcome memorization strategies and learn genuinely compositional rules. This approach leads to data-efficient, out-of-distribution generalization in cases where factorized latents alone would otherwise fail.

In addition, we provide in the Appendix A a general framework for interpreting compositionality and factorization that further clarifies these observations. Overall, these results caution against the assumption that a factorized bottleneck automatically confers compositional extrapolation, and they point toward more comprehensive design strategies for achieving genuinely compositional neural models.

2. Related Work

Disentangled Representation Learning. There is an extensive body of work on disentanglement, ranging from early theoretical proposals (Bengio et al., 2013) to various VAE-based approaches (e.g. β -VAE (Higgins et al., 2017a), FactorVAE (Kim & Mnih, 2018)) and GAN-based methods (Chen et al., 2016). Empirical metrics to quantify disentanglement include FactorVAE score, MIG score, and others (Eastwood & Williams, 2018). Yet, these often focus on axis-aligned or linear independence in the latent space, without explicitly evaluating compositional out-of-distribution performance. Indeed, (Locatello et al., 2019) show that unsupervised disentanglement is sensitive to inductive biases and data assumptions, raising questions about the connection to systematic compositional generalization.

Compositional Generalization & Disentanglement. Factorization and compositional generalization have been widely investigated in various architectures (Zhao et al., 2018; Higgins et al., 2017b; Burgess et al., 2018; Montero et al., 2021; Xu et al., 2022; Okawa et al., 2023; Wiedemer et al., 2023; Lippl & Stachenfeld, 2024; Liang et al., 2024b). For instance, Xu et al. (2022) introduced an evaluation protocol to assess compositional generalization in unsupervised representation learning, discovering that even well-disentangled representations do not guarantee improved out-of-distribution (OOD) behavior. Similarly, Montero et al. (2021) concluded that a model’s capacity to compose novel factor combinations can be largely decoupled from its degree of disentanglement. These observations temper the once-common assumption that factorized latents automati-

cally yield systematic compositional generalization. While many works study how β -VAEs and related methods learn disentangled representations (Burgess et al., 2018; Higgins et al., 2017a), they typically do not further explore the nuanced roles these representations play in compositional extrapolation—particularly in the presence of mixed discrete and continuous features. Consequently, a gap remains in understanding how—and to what extent—models that appear to disentangle latent factors can also robustly compose them under distribution shifts. Our work aims to illuminate this gap by investigating the detailed mechanics of factorization and compositionality within neural decoders, providing a complementary perspective to prior disentanglement benchmarks and broader generative modeling approaches.

3. Why Disentangled Bottlenecks Often Fail Compositional Generalization

We present a toy 2D Gaussian “bump” generation task that highlights a core phenomenon: even with explicitly disentangled inputs or bottleneck, standard feedforward networks can fail to generalize compositionally.

3.1. Toy Example: 2D Gaussian Bump Generation

Task Setup. We consider a generative model that receives a 2D coordinate (x, y) within some bounding box (e.g. $[0, N]^2$) and outputs a $N \times N$ grayscale image containing a Gaussian “bump” at location (x, y) . The in-distribution training set might cover an “O”-shaped region of (x, y) with a held-out OOD region in the center of the training distribution (Fig. 1(a)).

Architecture. In this work, we consider a scenario where an autoencoder’s latent bottleneck is explicitly regularized to learn a disentangled representation, and ask whether a decoder can truly leverage that factorization for compositional generalization. Concretely, we focus on a CNN-based “decoder-only” architecture that maps disentangled latent inputs to image outputs. We also experiment with MLP decoders and provide those results in Appendix E.3, observing similar qualitative findings.

Disentangled Input Encodings. Previous work has shown evidence indicating that vector-based representations are key to compositional generalization (Yang et al., 2023). Inspired by different forms of stimuli coding mechanisms within the biological brains (Georgopoulos et al., 1986; O’Keefe & Nadel, 1978; Shadlen & Newsome, 1998), we test various input encodings:

1. *Population-based coding*, e.g. a 1-hot, local-bump or positional encoding of x and y ,
2. *Rate-based coding*, a scalar (x, y) analog representation.

In each case, the input representation is trivially factorized

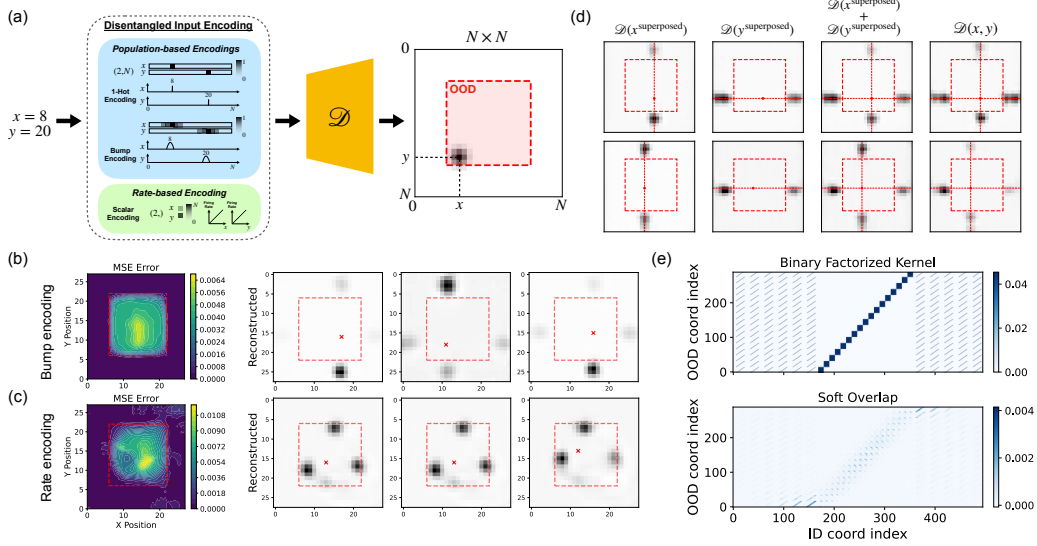


Figure 1. Various disentangled input encodings fail to support compositional generalization. (a) shows the experimental setup for the 2D Gaussian bump toy experiment, where the scalar (x, y) coordinate pair is encoded into disentangled representation (population-based vs. rate-based encodings), which is then fed to a decoder-only architecture to generate a $N \times N$ grayscale image of a single 2D Gaussian bump centered at that corresponding (x, y) location. The training dataset excludes all images that contain 2D Gaussian bumps centered within the red-shaded OOD region in the center of the image field. (b-c) shows the MSE error contour plots and sample generated OOD images of bump-based and rate-based encoding of the x and y input, the compositional OOD region is marked with by the red-dashed bounding box and the ground truth bump location is marked by a red cross. For a non-compositional network trained with bump-encoded inputs, (d) demonstrates that it learns to “superpose” seen ID training data when asked to compositionally generalize, and (e) shows the agreement between a theoretical binary factorized kernel with the similarity matrix (computed based on the pixel overlap) between the model’s ID and OOD generated samples.

w.r.t. x and y (meaning x and y are independently encoded by separate neurons). We then feed these inputs into a CNN that upsamples or decodes into an $N \times N$ image. For the remainder of the manuscript, we mostly compare and contrast models trained with the local-bump input encoding (x or y inputs embedded as the center of a 1D Gaussian bump, a vector of length N) and scalar input encoding (x or y inputs as scalar values).

3.2. Model fails to compositionally generalize for all disentangled encoding types.

Despite the factorized or “disentangled” input, the model *does not* automatically learn to generalize beyond the ID region. In many runs, the CNN effectively memorizes the training distribution and fails to correctly place the bump in the OOD region. Fig. 1(b-c) show the MSE error landscapes of generated images (from ground truth images) as well as their corresponding generated OOD images for models trained with the two different input encodings. While networks trained with different input encodings demonstrate different degrees of “local” generalization, all networks seem to consistently generate bizarre artifacts such as multiple bumps, which lend insights into the learned mode of “compositional” generalization of the network in relation to

memorization. Hence, simply providing factorized inputs, regardless of the form of encodings, does not suffice. The deeper layers can re-entangle x and y or rely on memorized local features, leading to poor compositional extrapolation. While not shown, we have also experimentally verified that models trained with 1-hot and positional input encodings also fail to compositionally generalize, despite their factorized structure. These findings confirm that factorization alone, regardless of the input/bottleneck encoding formats, is not sufficient for compositional generalization.

3.3. Model “superposes” seen data when asked to generalize.

From Fig. 1(b-c), we observe consistent OOD generation pattern across the bump-based and rate-based input encodings. We note that similar generating patterns have been reported for CNN-based Diffusion model (Liang et al., 2024a). The consistency of these patterns across input encoding formats and architectures indicate a shared underlying mechanism of model learning and generalization that we further characterize here.

Kernel-based approach to characterizing OOD generalization. One approach to characterizing model’s performance on unseen data is to characterize a kernel K :

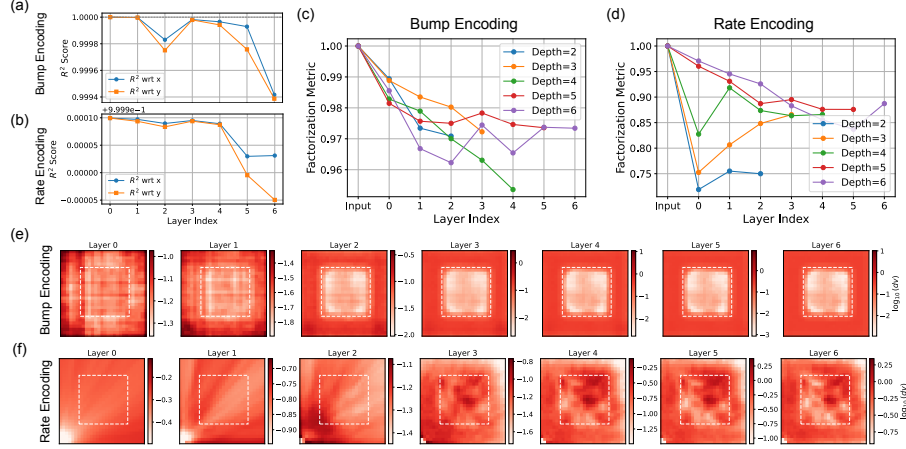


Figure 2. Failure of compositional generalization despite factorized input: input memorization undoes factorization. (a-b) show the linear probe metrics, and (c-d) show the factorization score (Eq. 7), and (e-f) show the volume metric $\log_{10}(dv)$, all as a function of layer depth, for models trained with bump-based vs. rate-based input encodings. The linear probe metric is defined as the R^2 scores of fitting two linear classifiers w.r.t. x and y .

$\mathcal{Z} \times \mathcal{Z} \rightarrow \mathbb{R}$, where $\mathcal{Z} = \mathcal{X} \times \mathcal{Y}$ is the cartesian product input domain of x and y coordinates of the Gaussian bumps in our toy example. Here we will focus our discussion to the 2-feature scenario for 2D Gaussian bump generation. A generalized introduction to kernel-based approach in characterizing factorization and OOD generalization is given in the Appendix A.4. We note that any positive-semidefinite, symmetric, and square-integrable kernel K can be decomposed into a Schmidt decomposition (for the 2-feature case):

$$K((x, y), (x', y')) = \sum_{r=1}^{\infty} \lambda_r k_x^{(r)}(x, x') k_y^{(r)}(y, y'), \quad (1)$$

where each term $k_x^{(r)}(x, x') k_y^{(r)}(y, y')$ is *rank-1* with respect to the (x) and (y) factors, and $\{\lambda_r\}$ are nonnegative eigenvalues. The number of terms with nonzero λ_k determines how mixed the kernel is. In practice, we can construct the discrete approximation, the *Gram matrix* \mathbf{K} on a finite set of data inputs $\{(x^{(i)}, y^{(i)})\}_{i=1}^M$ and their corresponding outputs:

$$\mathbf{K}_{(i,j)} = K((x^{(i)}, y^{(i)}), (x^{(j)}, y^{(j)})). \quad (2)$$

Non-compositional models learn a binary factorized kernel. In the kernel language, we would expect a compositional model to break down a novel input combination $(x, y)_{\text{OOD}}$ into factorized kernel, each independently mapping x and y to the seen components via K_x and K_y . From the generated OOD outputs of the networks shown in Fig. 1(b-c), we observe that the generated bumps seem to align with the ground truth x and y coordinates of the OOD bump. Empirically, we found that this is due to the model

memorizing the ID data and “superposing” activations corresponding all or some of the seen data of x and y when asked to generalize to $(x, y)_{\text{OOD}}$.

In Fig. 1(d), we show that the model’s output on a novel input pair $\mathcal{D}((x, y)_{\text{OOD}})$ is the combination of all of the model outputs with the “superposed” inputs, $x^{\text{superposed}} = (x, \sum_i^{M_{\text{ID}}} y^{(i)} / M_{\text{ID}})$ and similarly $y^{\text{superposed}} = (\sum_i^{M_{\text{ID}}} x^{(i)} / M_{\text{ID}}, y)$, i.e. $\mathcal{D}((x, y)_{\text{OOD}}) \approx \mathcal{D}(x^{\text{superposed}}) + \mathcal{D}(y^{\text{superposed}})$. Here M_{ID} is the number of ID data. To be more concrete, in the language of kernel, we can define a *binary factorized kernel*,

$$K_{\text{binary}}((x_i, y_i), (x_j, y_j)) = \kappa_x(x_i, x_j) \otimes_{\text{OR}} \kappa_y(y_i, y_j) \quad (3)$$

$$= \kappa_x(x_i, x_j) + \kappa_y(y_i, y_j) - \kappa_x(x_i, x_j) \kappa_y(y_i, y_j), \quad (4)$$

where $\kappa_x(x_i, x_j) = \kappa_y(y_i, y_j) = \delta_{i,j}$ is given by the Kronecker delta function. With normalization, the Gram matrix element is given by $\tilde{K}_{i,j} = \frac{K_{\text{binary}}(i,j)}{\sum_{j'} K_{\text{binary}}(i,j')}$. In Fig. 1(e), we show the agreement between the binary factorized kernel (top left) and the similarity matrix between the OOD and ID generated samples. This agreement shows that the factorized input structure is allowing the model to map x and y coordinates independently to ID samples. Nonetheless, the model fails to generalize OOD because it has not learned disentangled factors associated with either. A full kernel mapping between ID and OOD generated samples can be found in Appendix 8.

In a set of follow-up experiments on MNIST image rotation, we observe that this same “superposition” of memorized activation patterns—drawn from related in-distribution data—emerges as a general OOD generalization strategy in neural networks that have learned to memorize ID data.

Crucially, this phenomenon applies not only to compositional tasks but also to single-dimension interpolation and extrapolation. We detail these results in Appendix E.2.

3.4. Manifold warping through dimension expansion ruins factorization in latent space.

Why is disentangled input insufficient for learning disentangled factors of variation? Here we seek deeper mechanistic insights into model’s learned representations along the network layers. Specifically, we track how strongly x and y remain disentangled across layers. We find that while the *input* layer is trivially factorized, subsequent convolutional layers produce *mixed* features with large cross-terms, particularly near the final decoding. This “manifold warping” effectively destroys compositional structure, leaving the network reliant on patterns that do not extend to unseen (x, y) combinations.

A transport perspective. From a transport perspective, the model layers effectively learn to interpolate between the input (source) distribution and the output (target) distribution. Here the source distribution corresponds to the disentangled input representation manifold, while the output corresponds to the ID data representation manifold, which has an OOD “hole” in the middle. If there is nontrivial topological or geometrical deformation to the source or the target distribution representations, the model will have a hard time maintaining the integrity of the factorization, especially through dimension expansion (or reduction equivalently) in the generation process. Let the network be a composition of layers $T = T_L \circ \dots \circ T_1$, with each $T_l : \mathcal{Z}_{l-1} \rightarrow \mathcal{Z}_l$. The input measure μ_0 (assumed factorized) on \mathcal{Z}_0 is “pushed forward” through these layers to match the in-distribution measure μ_L^{ID} on the final space \mathcal{Z}_L . Formally, $\mu_l = (T_l \circ \dots \circ T_1)_* \mu_0$ for $l = 1, \dots, L$, so $\mu_L = T_* \mu_0$ should approximate μ_L^{ID} . If μ_L^{ID} differs topologically or geometrically from μ_0 (e.g. having an OOD “hole”), each layer T_l may need to warp coordinates significantly. These warping steps can easily re-entangle originally factorized inputs, leading to failures in OOD regions.

Characterization of manifold warping and factorization. To qualitatively investigate the warping and its effect on the factorization of the layer-wise representations, we compute the Jacobian-based metric tensor g , inspired by the approach of Ref. (Zavatone-Veth et al., 2023). The generalized definition can be found in Appendix B. In short, the metric tensor is defined by

$$g(x, y) = J(x, y)^\top J(x, y), \quad (5)$$

where J is the Jacobian matrix w.r.t. the different input feature dimension, which corresponds to x and y in our synthetic toy setting. We then visualize the volume metric

$$dv(x, y) = \sqrt{\det(g(x, y))} dx dy \quad (6)$$

for representation output at each of the network layer. The metric visualizations $\log_{10}(dv)$ are compared between networks with bump-based vs. rate-based encodings in Fig. 2(e) and (f). Visually, we observe significant distortion as a function of network depth, especially in the OOD region. To accompany the distortion analysis, we plot the linear probe metric (linear classifier R^2 w.r.t x and y) as well as the factorization metric proposed based g in Eq. (7) as a function of network depth in Fig. 2(a-d). Here the factorization metric is defined as

$$\text{Factorization}(g(x, y)) = 1 - \frac{|g_{xy}(x, y)|}{|g_{xx}(x, y)| + |g_{yy}(x, y)|}, \quad (7)$$

where g_{ij} ’s are the matrix elements of the 2×2 matrix g . We note that both metrics decay relatively gracefully over the layer depth for both networks with bump-based and rate-based input encodings. Intriguingly, shallow networks with rate-based encoding experiences a sharper drop in factorization. This is likely due to the higher demand for dimension expansion with the rate-based 2-neuron input, which leads to higher distortion when allowed fewer network layers to accommodate the expansion. The volume metric visualization as well as the linear probe metric as a function of layer depth for different network depths are shown in Fig. 11 and Fig. 12 (Fig. 13 and Fig. 14 for MLPs) as well as generated OOD images in Fig. 10 in Appendix E.3.

4. Encouraging Compositional Generalization

Given the above model failures, we ask: *Which architectural or training strategies can preserve factorization and yield robust compositional generalization?* We provide two promising avenues next.

4.1. Architecture and Regularization For Low-Rank Embeddings

One approach is to architecturally encourage an expansion of the abstract latent representations into 2D embedding filters, while applying explicit rank regularization during the learning of these expansions (illustrated in Fig. 3(a)). For example, Cichocki et al. (2009) show that applying tensor factorization constraints can reduce spurious cross-factor interactions. We add a matrix/tensor factorization penalty to a set of 2D embedding filters for each feature dimension, encouraging them to remain rank-limited. Briefly, to enforce factorization in each embedding matrix $W_{i,j}$, we adopt an SVD-like decomposition to each 2D input embedding filter:

$$W_{i,j} = \sum_{n=1}^r v_i^{(n)} \lambda^{(n)} u_j^{(n)}, \quad (8)$$

where r is an upper bound on the rank, $\lambda^{(n)}$ are scalar coefficients, and $v_i^{(n)}, u_j^{(n)}$ are row- and column-basis vectors.

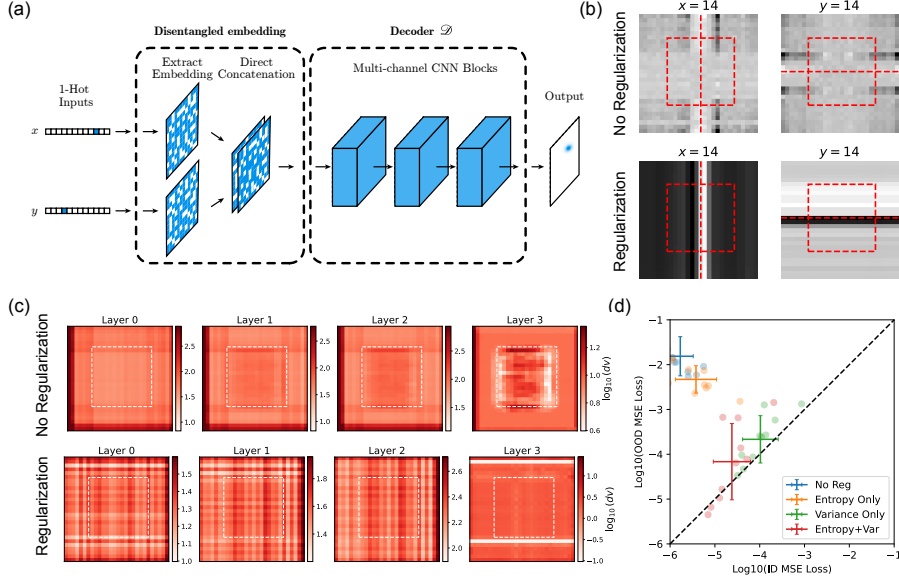


Figure 3. Inducing compositional generalization through architecture and regularization. (a) schematically illustrates the explicitly compositional architecture with factorized initial embedding layers for regularization (with 1-hot input encodings). (b) show sampled embedding activations corresponding to $x = 14$ and $y = 14$ for networks trained without and with regularization, respectively. (c) show the volume metric comparison between networks trained without and with regularization as a function of layer depth, respectively. (d) shows the OOD vs. ID MSE plot for various ablation studies over many runs.

To promote a low-rank and spatially consistent solution, we introduce entropy and variance penalties.

The squared magnitudes $[\lambda^{(n)}]^2$ define a probability distribution across n :

$$\tilde{\lambda}^{(n)} = \frac{[\lambda^{(n)}]^2}{\sum_{m=1}^r [\lambda^{(m)}]^2}, \quad (9)$$

which we regularize using an entropy penalty:

$$\mathcal{L}_{\text{ent}} = -\eta_1 \sum_{n=1}^r \tilde{\lambda}^{(n)} \ln \tilde{\lambda}^{(n)}, \quad (10)$$

encouraging dominance of only a few modes to enforce low rank.

Additionally, to discourage memorization of individual indices, we penalize variance in $v^{(n)}$ and $u^{(n)}$:

$$\mathcal{L}_{\text{var}} = \eta_2 \sum_{n=1}^r \left[\text{Var}(v^{(n)}) + \text{Var}(u^{(n)}) \right]. \quad (11)$$

The total loss function combines these terms with standard reconstruction loss:

$$\mathcal{L}_{\text{total}} = \mathcal{L}_{\text{MSE}} + \mathcal{L}_{\text{ent}} + \mathcal{L}_{\text{var}}. \quad (12)$$

Applying these regularizations to the embedding matrices of both x - and y -factors results in more structured and factorized representations, improving generalization to unseen

coordinate pairs. Fig. 3(b) illustrates that, without regularization, the model struggles to preserve signal integrity in OOD regions. With regularization, the embeddings exhibit structured banding aligned with coordinate axes, indicating a discovered factorized representation beneficial for compositional extrapolation. In addition, Fig. 3(c) show that with regularization, the learned representation is significantly smoother than without, despite having the same factorized embedding architecture. Both results show

Ablation. To assess the impact of our regularization strategy, we compare four configurations: (1) *No Reg* (baseline MSE loss), (2) *Entropy Only* (applying Eq. (10)), (3) *Variance Only* (applying Eq. (11)), and (4) *Entropy+Var* (combining both). Fig. 3(d) plots in-distribution (ID) vs. out-of-distribution (OOD) MSE. The *No Reg* condition yields the lowest ID error but highest OOD error, reflecting poor generalization. *Entropy Only* marginally improves OOD performance, while *Variance Only* significantly enhances extrapolation at the cost of higher ID loss. Combining both constraints (*Entropy+Var*) achieves the best OOD performance while maintaining low ID error, striking the optimal balance for robust factorization.

Intuitively, the regularization leverages *simple, low-dimensional structure* in the learned embedding matrices. By limiting the effective rank, it forces the network to represent each factor (e.g. a coordinate dimension) through a small set of shared directions rather than separately mem-

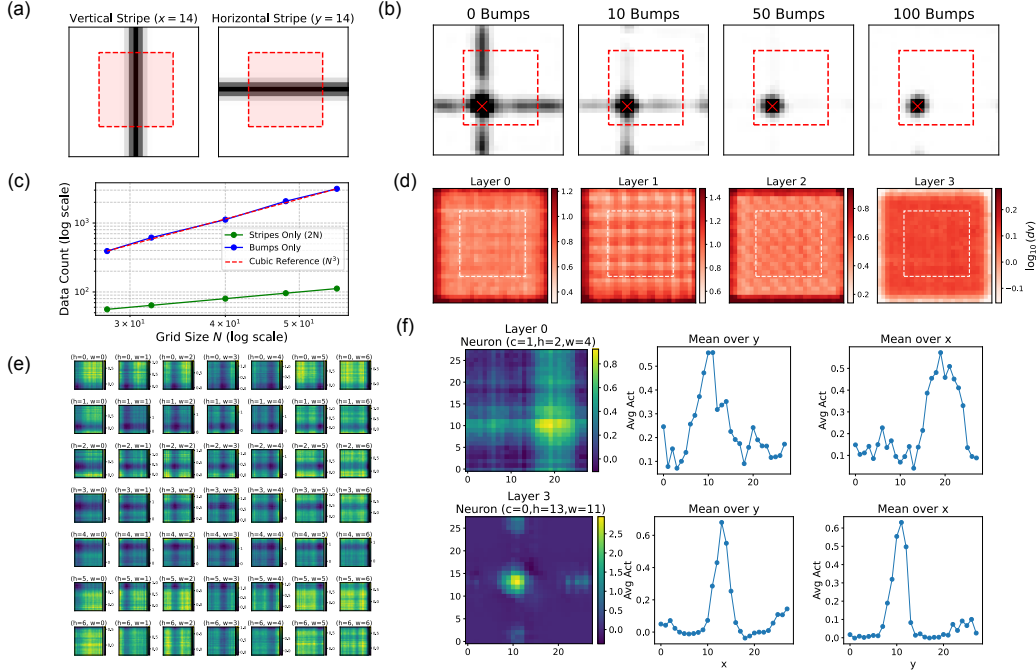


Figure 4. Inducing generalizable composition through training on independent factors. (a) show sample grayscale images of 1D Gaussian “stripes” at $x = 14$ and $y = 14$. (b) shows the generated OOD output as a function of number of Gaussian bumps included in the training dataset. (c) shows the data efficiency scaling of the stripes-only ($2N$) vs. bumps-only (N^3) to reach 90% accuracy of x and y generation as a function of image size N (accuracy assessed based on the location of the darkest pixel). Here stripes-only dataset has $2N$ scaling due to its ability to compositionally generalize zero-shot. (d) show the volume metric as a function of layer depth of the network trained on a dataset of stripes + bumps. (e) shows the 2D neuron activations across different channels in the first layer (layer 0) of a network trained on a dataset of stripes + 50 bumps. (f) shows neural tuning curves of two sample neurons at layer 0 and layer 3 of the same network as in (e).

orizing every possible input combination. Consequently, once the model learns an appropriate low-rank basis for in-distribution data, it can more easily *compose* those basis elements to handle new, unseen factor combinations in the OOD region. In other words, restricting the embedding to a few dominant modes discourages the network from relying on specific entries for every (x, y) , thereby reducing overfitting and promoting a genuinely factorized representation that better generalizes to novel coordinates.

4.2. Dataset Augmentation

Another approach that successfully enabled compositional generalization in the toy setting is dataset curation. Providing independent factors of variation in the form of x “stripes” and separate y stripes help the network discover a representation that enables composition.

Concretely, we generate 1D *vertical* and *horizontal* stripes by fixing a single coordinate (either x or y) and applying a 1D Gaussian in the orthogonal direction (samples shown in Fig. 4(a), full set shown in Fig. 7(a)). These stripes in the full output representational space act as building blocks that allow the network to learn each factor of variation *in-*

dependently in a way that abstract factorized inputs were not able to do. Optionally, we additionally include a small number of the 2D bumps (outside the OOD region, as before) in the training set, so the model also sees a small number of 2D examples. Consequently, the network acquires strong *compositional* ability: it generalizes to novel (x, y) -combinations outside the original training distribution (even with zero 2D bumps). Empirically, as demonstrated in Fig. 4, this approach markedly improves extrapolation performance.

Data efficiency scaling. Remarkably, we observed that models trained on a dataset consisting of just the stripes are able to compositionally generalize to generate additive stripe conjunctions in the OOD region without having seen any compositional examples (inside or outside the OOD region) during training, as shown in Fig. 4(b) when 0 2D Gaussian bump images are included in the training dataset. The remaining panels of Fig. 4(b) show that as we increase the number of 2D Gaussian bump images included in the training dataset, the model learns to generate proper bumps in the OOD region (also see Fig. 7(b)). We further characterize the data efficiency of such an approach of learning to compo-

sitionally generate bumps in the OOD region (learning with stripes + bumps) *versus* a traditional approach of learning with just bumps. Here we benchmark the compared models based on the minimal threshold amount of data needed to reach a target accuracy of 90% in generating the correct x and y coordinates of the stripe conjunctions/bumps. To our surprise, we found that models trained on datasets consisting of purely bumps has a data threshold that scales as the cube of the per-side image size, hence data requirements grow as the cube of the problem size, N . On the other hand, due to the zero-shot generalization capability of models trained on the stripe dataset, the scaling is linear with N , as the dataset consists of $2N$ stripes in total, N for x and N for y (together with 0 or a small number of bumps).

For comparison with the earlier results, we again plotted the volume metrics for the model trained on stripes + bumps dataset, as a function of model layer depth. The representations remain relatively smooth and uniform even across the OOD region, in contrast to the models trained with just the bumps shown in Fig. 2. In addition, we show in Fig. 4(e) the 2D activations of neurons in the first layer of a network trained on a dataset of stripes + 50 bumps. The activations show consistent “stripe” patterns that resemble the embeddings shown in Fig. 3(b) with regularization. Moreover, we show neural tuning curves w.r.t. to x and y for two sample neurons in layer 0 and layer 3 of the same network in Fig. 4(f), which exhibits “stripes” in early layers, which localizes to become a “bump” in downstream layers (more sample neural tuning curve can be found in Fig. 15).

Intuitively, these stripes provide a “scaffold” in the output space that is straightforward for the network to learn via additive composition. The model then leverages this scaffold to handle the more complex multiplicative compositional task—namely, generating intersections instead of mere unions—thereby achieving efficient bump generalization in the compositional OOD region. This highlights the value of *data-centric* strategies that emphasize the generative factors in isolation, consistent with the finding that dataset augmentation with stripes also improves compositional generalization and data-efficiency scaling for 2D bump generation in diffusion models in Ref. (Liang et al., 2024b).

Summary. The commonality in the two disparate methods that enable compositional generalization is that they both encourage factorization directly at the level of the 2D image space. By contrast, even directly supplying the network with factorized representations does not work if those representations are abstract and in a different space than the 2D image space. Our findings indicate that factorization learned in a latent space may not survive through subsequent dimension expansion in a decoder. Instead, to achieve robust compositional generalization, we found that it was important to

explicitly build or demonstrate factorization represented in the model’s *output space*. By ensuring that the network learns to separate each underlying factor (e.g. x and y) at the pixel level, we preserve the necessary compositional structure for strong extrapolation to novel conditions.

5. Discussion & Conclusion

Our results highlight two overarching principles:

1. **Disentangled latents are not enough.** Simply factorizing a single layer (e.g. the bottleneck) does not guarantee compositional structure in deeper layers; manifold warping can re-entangle factors and fail in OOD regions.
2. **Enforcing factorization in the output space is key.** Through explicit low-rank regularization or domain-centric augmentation (adding 1D stripes), we can maintain separable x/y embeddings and achieve strong extrapolation. In other words, building or preserving factorized structure across the entire model forward pass is essential for truly compositional generalization.

Limitations & Future Directions. While our investigation provides a clean, mechanistic view of why disentangled representations often fail on a synthetic 2D bump task, its scope is inherently limited by the toy nature of the setting. Extending these insights to large-scale models (e.g. Transformers, auto-regressive architectures) and high-dimensional data (vision, language) is an important next step to see whether similar re-entanglement dynamics persist. Furthermore, modern architectures like vision transformers or large language models may already embed implicit factorization biases (e.g. through attention or prompt-based modularity); rigorously assessing whether these biases genuinely promote compositional generalization would sharpen our understanding of inductive bias design. Finally, new metrics or frameworks are needed to capture *partial* and *hierarchical* compositional structures, since real-world tasks rarely exhibit a single, strict factorization. We provide a preliminary attempt for characterizing such partial factorization in Appendix A. By developing principled ways to quantify such subtler forms of compositionality, future work can more precisely guide architectural choices and regularization strategies toward robust OOD performance in more complex, real-world domains.

Ultimately, bridging the gap between *disentangled representations* and *compositional generalization* requires a holistic view of how a network’s *entire* forward pass maintains or destroys factorization. We hope this work provides a step toward that goal, clarifying both the pitfalls of standard bottleneck-based approaches and the promise of structural or regularized solutions.

Acknowledgements

The authors would like to thank Alan (Junzhe) Zhou, Ziming Liu, Federico Claudi, Megan Tjandrasuwita, Mitchell Ostrow, Sarthak Chandra, Ling Liang Dong, Hao Zheng, Tomaso Poggio, Cheng Tang for helpful discussions and feedback at various stages of this work.

References

- Bengio, Y., Courville, A. C., and Vincent, P. Representation learning: A review and new perspectives. *IEEE Trans. Pattern Anal. Mach. Intell.*, 35(8):1798–1828, 2013. doi: 10.1109/TPAMI.2013.50. URL <https://doi.org/10.1109/TPAMI.2013.50>.
- Burgess, C. P., Higgins, I., Pal, A., Matthey, L., Watters, N., Desjardins, G., and Lerchner, A. Understanding disentangling in β -vae. *CoRR*, abs/1804.03599, 2018. URL <http://arxiv.org/abs/1804.03599>.
- Chen, T. Q., Li, X., Grosse, R. B., and Duvenaud, D. Isolating sources of disentanglement in variational autoencoders. In Bengio, S., Wallach, H. M., Larochelle, H., Grauman, K., Cesa-Bianchi, N., and Garnett, R. (eds.), *Advances in Neural Information Processing Systems 31: Annual Conference on Neural Information Processing Systems 2018, NeurIPS 2018, December 3-8, 2018, Montréal, Canada*, pp. 2615–2625, 2018. URL <https://proceedings.neurips.cc/paper/2018/hash/1ee3dfcd8a0645a25a35977997223d22-Abstract.html>.
- Chen, X., Duan, Y., Houthooft, R., Schulman, J., Sutskever, I., and Abbeel, P. Infogan: Interpretable representation learning by information maximizing generative adversarial nets. In Lee, D. D., Sugiyama, M., von Luxburg, U., Guyon, I., and Garnett, R. (eds.), *Advances in Neural Information Processing Systems 29: Annual Conference on Neural Information Processing Systems 2016, December 5-10, 2016, Barcelona, Spain*, pp. 2172–2180, 2016. URL <https://proceedings.neurips.cc/paper/2016/hash/7c9d0b1f96aebd7b5eca8c3edaa19ebb-Abstract.html>.
- Cichocki, A., Zdunek, R., Phan, A. H., and Amari, S. *Nonnegative Matrix and Tensor Factorizations - Applications to Exploratory Multi-way Data Analysis and Blind Source Separation*. Wiley, 2009. ISBN 978-0-470-74666-0. doi: 10.1002/9780470747278. URL <https://doi.org/10.1002/9780470747278>.
- DeMoss, B., Sapora, S., Foerster, J. N., Hawes, N., and Posner, I. The complexity dynamics of grokking. *CoRR*, abs/2412.09810, 2024. doi: 10.48550/ARXIV.2412.09810. URL <https://doi.org/10.48550/arXiv.2412.09810>.
- Eastwood, C. and Williams, C. K. I. A framework for the quantitative evaluation of disentangled representations. In *6th International Conference on Learning Representations, ICLR 2018, Vancouver, BC, Canada, April 30 - May 3, 2018, Conference Track Proceedings*. OpenReview.net, 2018. URL <https://openreview.net/forum?id=By-7dz-AZ>.
- Ganin, Y., Ustinova, E., Ajakan, H., Germain, P., Larochelle, H., Laviolette, F., Marchand, M., and Lempitsky, V. S. Domain-adversarial training of neural networks. In Csurka, G. (ed.), *Domain Adaptation in Computer Vision Applications*, Advances in Computer Vision and Pattern Recognition, pp. 189–209. Springer, 2017. doi: 10.1007/978-3-319-58347-1_10. URL https://doi.org/10.1007/978-3-319-58347-1_10.
- Georgopoulos, A. P., Schwartz, A. B., and Kettner, R. E. Neuronal population coding of movement direction. *Science*, 233(4771):1416–1419, 1986. doi: 10.1126/science.3749889.
- Higgins, I., Matthey, L., Pal, A., Burgess, C. P., Glorot, X., Botvinick, M. M., Mohamed, S., and Lerchner, A. beta-vae: Learning basic visual concepts with a constrained variational framework. In *5th International Conference on Learning Representations, ICLR 2017, Toulon, France, April 24-26, 2017, Conference Track Proceedings*. OpenReview.net, 2017a. URL <https://openreview.net/forum?id=Sy2fzU9gl>.
- Higgins, I., Matthey, L., Pal, A., Burgess, C. P., Glorot, X., Botvinick, M. M., Mohamed, S., and Lerchner, A. beta-vae: Learning basic visual concepts with a constrained variational framework. In *5th International Conference on Learning Representations, ICLR 2017, Toulon, France, April 24-26, 2017, Conference Track Proceedings*. OpenReview.net, 2017b. URL <https://openreview.net/forum?id=Sy2fzU9gl>.
- Kim, H. and Mnih, A. Disentangling by factorising. In Dy, J. G. and Krause, A. (eds.), *Proceedings of the 35th International Conference on Machine Learning, ICML 2018, Stockholmsmässan, Stockholm, Sweden, July 10-15, 2018*, volume 80 of *Proceedings of Machine Learning Research*, pp. 2654–2663. PMLR, 2018. URL <http://proceedings.mlr.press/v80/kim18b.html>.
- Lake, B. M. and Baroni, M. Generalization without systematicity: On the compositional skills of sequence-to-sequence recurrent networks. In Dy, J. G. and Krause, A. (eds.), *Proceedings of the 35th International Conference on Machine Learning, ICML 2018, Stockholmsmässan, Stockholm, Sweden, July 10-15, 2018*, volume 80 of *Proceedings of Machine Learning Research*, pp. 2879–2888. PMLR, 2018. URL <http://proceedings.mlr.press/v80/lake18a.html>.

- Liang, Q., Liu, Z., and Fiete, I. R. Do diffusion models learn semantically meaningful and efficient representations? In *ICLR 2024 Workshop on Mathematical and Empirical Understanding of Foundation Models*, 2024a. URL <https://openreview.net/forum?id=pAAMFQiAuD>.
- Liang, Q., Liu, Z., Ostrow, M., and Fiete, I. How diffusion models learn to factorize and compose. In *38th Conference on Neural Information Processing Systems, NeurIPS 2024*, 2024b.
- Lippl, S. and Stachenfeld, K. When does compositional structure yield compositional generalization? A kernel theory. *CoRR*, abs/2405.16391, 2024. doi: 10.48550/ARXIV.2405.16391. URL <https://doi.org/10.48550/arXiv.2405.16391>.
- Locatello, F., Bauer, S., Lucic, M., Rätsch, G., Gelly, S., Schölkopf, B., and Bachem, O. Challenging common assumptions in the unsupervised learning of disentangled representations. In Chaudhuri, K. and Salakhutdinov, R. (eds.), *Proceedings of the 36th International Conference on Machine Learning, ICML 2019, 9-15 June 2019, Long Beach, California, USA*, volume 97 of *Proceedings of Machine Learning Research*, pp. 4114–4124. PMLR, 2019. URL <http://proceedings.mlr.press/v97/locatello19a.html>.
- Montero, M. L., Ludwig, C. J. H., Costa, R. P., Malhotra, G., and Bowers, J. S. The role of disentanglement in generalisation. In *9th International Conference on Learning Representations, ICLR 2021, Virtual Event, Austria, May 3-7, 2021*. OpenReview.net, 2021. URL <https://openreview.net/forum?id=qBH974jKUVy>.
- Okawa, M., Lubana, E. S., Dick, R. P., and Tanaka, H. Compositional abilities emerge multiplicatively: Exploring diffusion models on a synthetic task. *CoRR*, abs/2310.09336, 2023. doi: 10.48550/ARXIV.2310.09336. URL <https://doi.org/10.48550/arXiv.2310.09336>.
- O’Keefe, J. and Nadel, L. *The Hippocampus as a Cognitive Map*. Oxford University Press, Oxford, UK, 1978.
- Shadlen, M. N. and Newsome, W. T. The variable discharge of cortical neurons: implications for connectivity, computations, and coding. *The Journal of Neuroscience*, 18(10):3870–3896, 1998. doi: 10.1523/JNEUROSCI.18-10-03870.1998.
- Wiedemer, T., Mayilvahanan, P., Bethge, M., and Brendel, W. Compositional generalization from first principles. In Oh, A., Naumann, T., Globerson, A., Saenko, K., Hardt, M., and Levine, S. (eds.), *Advances in Neural Information Processing Systems 36: Annual Conference on Neural Information Processing Systems 2023, NeurIPS 2023, New Orleans, LA, USA, December 10 - 16, 2023*, 2023. URL http://papers.nips.cc/paper_files/paper/2023/hash/15f6a10899f557ce53fe39939af6f930-Abstract-Conference.html.
- Xu, Z., Niethammer, M., and Raffel, C. Compositional generalization in unsupervised compositional representation learning: A study on disentanglement and emergent language. In Koyejo, S., Mohamed, S., Agarwal, A., Belgrave, D., Cho, K., and Oh, A. (eds.), *Advances in Neural Information Processing Systems 35: Annual Conference on Neural Information Processing Systems 2022, NeurIPS 2022, New Orleans, LA, USA, November 28 - December 9, 2022*, 2022. URL http://papers.nips.cc/paper_files/paper/2022/hash/9f9ecbf4062842df17ec3f4ea3ad7f54-Abstract-Conference.html.
- Yang, T., Wang, Y., Lan, C., Lu, Y., and Zheng, N. Vector-based representation is the key: A study on disentanglement and compositional generalization. *CoRR*, abs/2305.18063, 2023. doi: 10.48550/ARXIV.2305.18063. URL <https://doi.org/10.48550/arXiv.2305.18063>.
- Zavatone-Veth, J. A., Yang, S., Rubinien, J. A., and Pehlevan, C. Neural networks learn to magnify areas near decision boundaries. *CoRR*, abs/2301.11375, 2023. doi: 10.48550/ARXIV.2301.11375. URL <https://doi.org/10.48550/arXiv.2301.11375>.
- Zhao, S., Ren, H., Yuan, A., Song, J., Goodman, N. D., and Ermon, S. Bias and generalization in deep generative models: An empirical study. In Bengio, S., Wallach, H. M., Larochelle, H., Grauman, K., Cesa-Bianchi, N., and Garnett, R. (eds.), *Advances in Neural Information Processing Systems 31: Annual Conference on Neural Information Processing Systems 2018, NeurIPS 2018, December 3-8, 2018, Montréal, Canada*, pp. 10815–10824, 2018. URL <https://proceedings.neurips.cc/paper/2018/hash/5317b6799188715d5e00a638a4278901-Abstract.html>.

A. A Framework for Compositionality, Factorization, and Modularity

Existing literature is divided on whether disentangled representation learning truly fosters compositional generalization and data efficiency. Despite extensive empirical studies and numerous proposed metrics, there is still no unified framework that clearly defines factorization, disentanglement, and compositionality or their interrelationships. A key challenge lies in the lack of a systematic “language” to characterize the various types and degrees of these concepts. Furthermore, real-world datasets often exhibit multiple, overlapping forms of compositionality, each with its own failure modes that can obscure one another. In response, we aim to develop a more general framework that makes these distinctions explicit.

This section aims to establish a framework for unifying the concepts of compositionality, factorization, disentanglement, and modularity. Specifically, we introduce two core components of our framework. First, we define the *compositional complexity* of a target function or distribution via the minimal number of rank-1 product terms needed to represent it. Then, we formalize *factorization* (disentanglement) for the intermediate activations of a neural network, allowing for arbitrary invertible transformations.

A.1. Definition of compositionality and compositional complexity

Here we take on a function learning perspective of defining factorization and compositionality. Specifically, for learning a compositional solution, we expect network to first learn how to “break down” (factorize) component factors and then flexibly “re-combine” them for compositional generation. For a neural network learning a generic N -way composite target function $f : \mathcal{X}_1 \times \dots \times \mathcal{X}_N \rightarrow \mathbb{R}^M$ of N features $\{x_1, x_2, \dots, x_N\}$, we can write the tensor decomposition of this function as

$$f(x_1, \dots, x_N) = \sum_{r=1}^R \lambda_r \phi_r^{(x_1)}(x_1) \cdots \phi_r^{(x_N)}(x_N), \quad (13)$$

where $\phi_r^{(x_i)}(x_i) : \mathcal{X}_i \rightarrow \mathbb{R}^M$ and $\lambda_i \in \mathbb{R}$ are lumped factors.

Note that this decomposition is not unique, meaning that a given function f might permit multiple degenerate decomposition with the same rank or different ranks. This means that the network is not guaranteed to learn a compositional decomposition that aligns with the canonical axes of variation, as required by some of the disentanglement metrics in existing literature.

Probability Distributions as a Sum of Product Factors. In some settings, rather than learning a deterministic function $f : \mathcal{X}_1 \times \dots \times \mathcal{X}_N \rightarrow \mathbb{R}^M$, we aim to model a *joint probability distribution* $p(x_1, \dots, x_N)$. An analogous “sum-of-products” factorization can be written as:

$$p(x_1, \dots, x_N) = \sum_{r=1}^R \lambda_r p_1^{(r)}(x_1) \cdots p_N^{(r)}(x_N), \quad \text{with} \quad \sum_{r=1}^R \lambda_r = 1, \quad \lambda_r \geq 0. \quad (14)$$

Here, each $p_i^{(r)}(x_i)$ denotes a univariate (or lower-dimensional) distribution on \mathcal{X}_i , and λ_r are nonnegative mixture weights. In discrete domains, $p_i^{(r)}$ can be categorical distributions; in continuous domains, they can be densities (e.g. Gaussian components or neural-network-based PDFs). Intuitively, we are representing p as a *mixture* of “fully factorized” product distributions, each contributing a rank-1 tensor $p_1^{(r)} \times \dots \times p_N^{(r)}$ in the joint space.

Defining Compositional Complexity. There are some compositional functions or probability distributions that are inherently more difficult to learn than others. Here we formalize the “compositional complexity” of a target function or distribution via the minimal number of rank-1 (factorized) terms required in a sum-of-product decomposition. Let N be the number of factors (or dimensions), and let $\{\phi_r^{(x_i)}\}$ or $\{p_i^{(r)}\}$ denote per-factor functions or distributions.

Case 1: Deterministic Function. For $f : \mathcal{X}_1 \times \dots \times \mathcal{X}_N \rightarrow \mathbb{R}^M$, assume $M = 1$ for simplicity, or treat each output dimension independently. A sum-of-product (CP) representation is

$$f(x_1, \dots, x_N) = \sum_{r=1}^R \prod_{i=1}^N \phi_r^{(x_i)}(x_i), \quad (\text{up to a scalar factor } \lambda_r \text{ if desired}). \quad (15)$$

Define the *exact rank* of f as:

$$R^*(f) = \min \left\{ R \mid f(x_1, \dots, x_N) = \sum_{r=1}^R \prod_{i=1}^N \phi_r^{(x_i)}(x_i) \right\}. \quad (16)$$

If f cannot be exactly decomposed with finite R , we consider an ε -approximation in some norm or error measure $\|\cdot\|$:

$$R_\varepsilon^*(f) = \min \left\{ R \mid \left\| f - \sum_{r=1}^R \prod_{i=1}^N \phi_r^{(x_i)}(x_i) \right\| \leq \varepsilon \right\}. \quad (17)$$

A smaller $R^*(f)$ (or $R_\varepsilon^*(f)$) indicates f is more “compositional” or factorized.

Case 2: Probability Distribution. For a joint probability $p(x_1, \dots, x_N)$, a sum-of-products corresponds to a finite mixture of product distributions:

$$p(x_1, \dots, x_N) = \sum_{r=1}^R \lambda_r \prod_{i=1}^N p_i^{(r)}(x_i), \quad \sum_{r=1}^R \lambda_r = 1, \quad \lambda_r \geq 0. \quad (18)$$

Its *exact rank* is:

$$R^*(p) = \min \left\{ R \mid p = \sum_{r=1}^R \lambda_r \prod_{i=1}^N p_i^{(r)}(x_i) \right\}. \quad (19)$$

If no finite R yields an exact factorization, we allow an ε -approximation w.r.t. a suitable divergence $D(\cdot, \cdot)$ (e.g. KL divergence or total variation distance):

$$R_\varepsilon^*(p) = \min \left\{ R \mid D\left(p \parallel \sum_{r=1}^R \lambda_r \prod_{i=1}^N p_i^{(r)}(x_i)\right) \leq \varepsilon \right\}. \quad (20)$$

Again, smaller ranks correspond to “low compositional complexity” (fewer factorized terms), whereas large R indicates more intricate cross-factor entanglements.

A.2. Definition of Factorization/Disentanglement of Neural Networks

Having introduced the notion of *intrinsic compositionality* for a target function or distribution, we now shift to defining *factorization* (a.k.a. disentanglement) in the context of a neural network’s activation space. This concept applies to an intermediate layer or the entire network.

Defining factorization vs. disentanglement. Despite the frequent usage of these terms, there is no universal consensus on their precise definitions in the literature. Some works treat them as strictly synonymous, while others reserve “factorization” for representations whose coordinates directly correspond to physically or semantically independent factors (e.g. each latent dimension controlling one ground-truth variable). By contrast, “disentanglement” can refer to a broader class of methods or criteria (e.g. axis-aligned independence, mutual information scores, or partial correlations). In this paper, we do not distinguish sharply between these nuances. Wherever we refer to “disentangled” or “factorized” representations, we mean that a model’s latent (or intermediate) dimensions reflect independently varying components of the data. The specific implementation details—whether formalized via a β -VAE objective, mutual-information measures, or other constraints—are secondary to the overall idea that each latent dimension ideally captures a different underlying factor. Hence, we use the two terms *interchangeably* throughout the manuscript.

Activation Matrix Setup. Let

$$\alpha : \mathcal{X}_1 \times \dots \times \mathcal{X}_N \rightarrow \mathbb{R}^D \quad (21)$$

represent the activations of a given network layer. For an input (x_1, \dots, x_N) , the output $\alpha(x_1, \dots, x_N) \in \mathbb{R}^D$. Over N_{ID} training samples $\{(x_{1,i}, \dots, x_{N,i})\}_{i=1}^{N_{\text{ID}}}$, we can assemble an activation matrix

$$\alpha \in \mathbb{R}^{N_{\text{ID}} \times D}, \quad \text{where row } i \text{ is } \alpha(x_{1,i}, \dots, x_{N,i}). \quad (22)$$

Optionally, we may project α to a lower dimension $K \leq D$ via $W \in \mathbb{R}^{K \times D}$ (e.g. PCA), yielding

$$\alpha_{\text{feat}}(x_1, \dots, x_N) = \alpha(x_1, \dots, x_N) W^\top \in \mathbb{R}^K. \quad (23)$$

General Definition of Factorization. A purely linear test might require an invertible matrix $U \in \mathbb{R}^{K \times K}$ such that

$$\alpha_{\text{feat}}(x_1, \dots, x_N) U^\top = [\beta_1(x_1), \dots, \beta_N(x_N)], \quad (24)$$

where each block of coordinates depends *only* on a single factor x_j . However, factorization may emerge only under a *nonlinear* reparametrization. Hence, we relax the requirement to any invertible map

$$T : \mathbb{R}^D \rightarrow \mathbb{R}^D \quad (\text{e.g. a diffeomorphism or normalizing flow}). \quad (25)$$

Definition (General Factorization). We say $\alpha : \mathcal{X}_1 \times \dots \times \mathcal{X}_N \rightarrow \mathbb{R}^D$ is *nonlinearly factorized* w.r.t. (x_1, \dots, x_N) if there exist:

1. An invertible transformation $T : \mathbb{R}^D \rightarrow \mathbb{R}^D$,
2. A partition of $\{1, \dots, D\}$ into N disjoint subsets $I_1 \cup \dots \cup I_N$,

such that defining

$$\beta(x_1, \dots, x_N) = T(\alpha(x_1, \dots, x_N)) \in \mathbb{R}^D, \quad (26)$$

we have, for every coordinate $i \in I_j$,

$$\beta_i(x_1, \dots, x_N) = \beta_i(x_j) \quad \text{depends only on } x_j. \quad (27)$$

Concretely, in these transformed coordinates $(\beta_1, \dots, \beta_N)$, each subset of coordinates implements the feature(s) of a single factor x_j , with *no cross-dependence* among different factors.

Modularity via Factorization. A representation is *functionally modular* if, under some invertible transform T , we can rearrange the coordinates into sub-blocks that each depend on exactly one factor x_j . This directly matches the factorization criterion above. In contrast, a *structurally modular* network places each factor’s neurons in physically separate submodules (e.g. block-diagonal connectivity), making the separation visible *without* any transform. Hence, functional modularity (factorization) is more general and only requires a suitable reparametrization in \mathbb{R}^D , whereas structural modularity is a stricter design property at the raw parameter level.

A.3. Partial Factorization, Entanglement, and Reversibility

Sections A.2 gave a definition of factorization vs. entanglement: if *any* invertible map T can reorder the coordinates into blocks that depend purely on x or purely on y , we call the representation factorized; otherwise, it is entangled. In practice, however, real-world data and deep networks often produce *partial* factorization, where some features mix x and y only mildly or separate them only in certain regions. Further, certain layers introduce *irreversible* steps (e.g. pooling, saturations), which can destroy factor structure. We elaborate on these points below.

Partial Factorization. A representation need not split perfectly into two blocks (I_x and I_y) to convey some compositional benefits. For example, consider a multi-factor domain (x, y, z) in which the representation merges two of the factors (x, y) but leaves z separate. One might say the network has *partially factorized* the input. More formally, partial factorization arises if *some* invertible map T can partition the D coordinates into sub-blocks, each depending on a subset (not necessarily size 1) of the factors. This differs from pure factorization in that each block may mix more than one factor, yet remain independent of other blocks. Concretely:

$$T(\alpha(x, y, z)) = [\beta_{xy}(x, y), \beta_z(z)], \quad \text{with minimal cross-dependence among blocks.} \quad (28)$$

This partial structure still yields some compositional benefits (e.g. reusing the (x, y) sub-block in new contexts of z). But it may not qualify as fully “disentangled” in the strict sense of Section A.2. Indeed, such partial factorization commonly appears if x and y are correlated in training data or if the network’s architecture merges them early.

Entanglement via Irreversible Mixing. Even if a representation starts factorized in an early layer, the network may subsequently *entangle* factors by applying irreversible operations such as:

- **Pooling or Striding:** Combining multiple spatial positions (or multiple channels) into one, discarding the ability to invert them individually.

- **Nonlinear Saturation:** A ReLU or sigmoid can “clip” signals, so the original amplitude differences from x vs. y can no longer be fully recovered.
- **Dimension Reduction:** Fully connected layers that collapse from a higher dimension D to a smaller one $D' < D$ can forcibly merge features.

Because our definition of factorization requires an *invertible* map T to unscramble the coordinates, any irreversible merge that loses information effectively prevents us from re-separating x and y . Thus, irreversible mixing is a key mechanism by which networks destroy factorization.

Reversible Mixing Need Not Break Factorization. By contrast, a *reversible* or *bijective* layer can combine factors in intermediate channels without permanently entangling them, so long as there exists an inverse transform. For instance, a normalizing-flow block may shuffle or mix (x, y) channels in a fully invertible manner; the overall system can still preserve factorization if the subsequent training does not “pinch” those degrees of freedom. In principle, any invertible map that merges coordinates can be “undone” later, so the final representation might remain factorized.

A.4. A Kernel-Based Perspective on Factorization

To operationalize the above definitions of factorization/disentanglement concretely, we here propose a kernel-based perspective and define a *factorization metric* that assess the factorization of the kernel learned by the neural network. The goal here is to characterize such a kernel, given its potentially factorized form, to understand the different regimes in which it compositionally generalize (or not).

We now consider an N -partite domain $\mathcal{X}_1 \times \cdots \times \mathcal{X}_N$ and a positive-semidefinite (PSD) kernel

$$K : (\mathcal{X}_1 \times \cdots \times \mathcal{X}_N) \times (\mathcal{X}_1 \times \cdots \times \mathcal{X}_N) \rightarrow \mathbb{R}. \quad (29)$$

Under suitable conditions (e.g. an analogue of Mercer’s theorem), K often admits a *sum-of-product* (canonical polyadic) expansion:

$$K\left((x_1, \dots, x_N), (x'_1, \dots, x'_N)\right) = \sum_{r=1}^{R^*} \lambda_r \prod_{j=1}^N k_j^{(r)}(x_j, x'_j), \quad (30)$$

where each term $\lambda_r \prod_{j=1}^N k_j^{(r)}(x_j, x'_j)$ is *rank-1* across the N factors, and R^* may be finite or infinite.

Interpretation. If $R^* = 1$ in (30), we say K is a *purely factorized* (rank-1) kernel, effectively separating each factor x_j . Larger $R^* > 1$ signals *partial* or *full* entanglement across these factors in K .

Rank-Based Measure of Factorization. We define the *CP rank* of K by

$$\text{rank}(K) = \min\{R^* \mid (30) \text{ holds exactly}\}, \quad (31)$$

in analogy to the Schmidt rank in bipartite systems. A small rank implies that K is closer to a “fully separable” structure across (x_1, \dots, x_N) , while a large rank means more cross-term mixing.

A.5. Polynomial Expansions and a Generalized Factorization Metric

Suppose K admits a polynomial-like expansion enumerating single-factor, pairwise, and higher-order cross terms:

$$K = \sum_{\ell} \theta_{\ell} K_{\ell}, \quad (32)$$

where each K_{ℓ} might be an n -factor product kernel on a subset of coordinates, and θ_{ℓ} is its coefficient. We assign each θ_{ℓ} a “weight” $w(\theta_{\ell})$, for instance $|\theta_{\ell}|$ or θ_{ℓ}^2 . A *generalized factorization metric* then measures the fraction of K ’s “weight” contributed by a chosen subset of “lower-order” terms. Formally, if \mathcal{S} denotes the subset of indices corresponding to single-factor (or low-order) terms, we define

$$\text{PF_Coeff}^{(\mathcal{S})}(K) = \frac{\sum_{\ell \in \mathcal{S}} w(\theta_{\ell})}{\sum_{\ell} w(\theta_{\ell})}. \quad (33)$$

By varying \mathcal{S} (e.g. only single-factor vs. single-plus-pairwise), we obtain a family of “explained fraction” values—analogueous to cumulative explained variance in PCA. A higher fraction indicates that K is dominantly factorized by low-order expansions (less entangled), whereas large higher-order terms imply more cross-variable mixing.

Operational Regimes of NNs in light of this decomposition. Based on the defined rank-based measure of factorization, we can imagine two operational regime limits of the neural networks, namely

- *Pure memorization regime:* in which case the network resorts to tabular learning (memorization), i.e. learning a single N -factor kernel term
- *Pure factorization regime:* in which case the network learns a completely compositional kernel (assuming each of the N factors are independent).

These are obviously theoretical limits, and in reality, the network probably operates in a regime that interpolates between the two, i.e. learning partially/imperfectly factorized solutions.

How to estimate this metric in practice. In real-world scenarios, we rarely have direct access to the continuous kernel $K : (\mathcal{X}_1 \times \dots \times \mathcal{X}_N)^2 \rightarrow \mathbb{R}$. Instead, we can discretize K by selecting a finite set of data points $\{(x_{1,i}, \dots, x_{N,i})\}_{i=1}^M$ and forming the $M \times M$ Gram matrix:

$$\mathbf{K}_{(i,j)} = K\left((x_{1,i}, \dots, x_{N,i}), (x_{1,j}, \dots, x_{N,j})\right). \quad (34)$$

We can interpret this matrix as a discrete approximation to K . To apply our *generalized factorization metric* (§A.5), we then:

1. **Approximate expansions.** Attempt to factor (or partially factor) \mathbf{K} into a sum-of-product form among the N factors, e.g. through low-rank tensor methods or suitable polynomial expansions on the sampled coordinates.
2. **Coefficient extraction.** If we assume a polynomial-like expansion, $\mathbf{K} \approx \sum_{\ell} \theta_{\ell} \mathbf{K}_{\ell}$, we obtain finite-dimensional coefficients $\{\theta_{\ell}\}$ by fitting or projecting onto a chosen basis.
3. **Compute the factorization ratio.** Restrict attention to the “low-order” terms (e.g. single-factor or pairwise) to form a subset \mathcal{S} . Define

$$\text{PF_Coeff}^{(\mathcal{S})}(\mathbf{K}) = \frac{\sum_{\ell \in \mathcal{S}} w(\theta_{\ell})}{\sum_{\ell} w(\theta_{\ell})}, \quad (35)$$

just as in the continuous setting, but now ℓ indexes a finite set of basis or fitted components.

This procedure yields a practical, data-driven measure of how “factorized” the *empirical kernel* is on the sampled domain. Notably, if the sampling is sparse or unrepresentative, the resulting \mathbf{K} may fail to capture subtle cross-factor structure. In that sense, one can view $\text{PF_Coeff}^{(\mathcal{S})}(\mathbf{K})$ as an *approximate* or *lower-dimensional* proxy for $\text{PF_Coeff}^{(\mathcal{S})}(K)$ in the continuous limit.

B. Metric Tensor and Factorization Metric for N -Dimensional Inputs

In this appendix, we outline a generic procedure to quantify the local geometry of a neural representation \mathbf{f} defined on an N -dimensional input space, with the metric tensor g from Ref. (Zavatone-Veth et al., 2023), and then specialize to the 2D case with an explicit factorization metric that we propose based on g .

B.1. General N -Dimensional Definition Representation and Jacobian.

$$\mathbf{f} : \mathbb{R}^N \rightarrow \mathbb{R}^D, \quad (36)$$

where $\mathbf{f}(x_1, \dots, x_N) = (f_1, \dots, f_D)$ for each input vector $\mathbf{x} = (x_1, \dots, x_N)$. We define the Jacobian J of \mathbf{f} at a point \mathbf{x} by

$$J(\mathbf{x}) = \begin{bmatrix} \partial f_1 / \partial x_1 & \cdots & \partial f_1 / \partial x_N \\ \vdots & \ddots & \vdots \\ \partial f_D / \partial x_1 & \cdots & \partial f_D / \partial x_N \end{bmatrix} \in \mathbb{R}^{D \times N}. \quad (37)$$

Metric Tensor. The induced *metric tensor* $g(\mathbf{x})$ is then an $N \times N$ matrix,

$$g(\mathbf{x}) = J(\mathbf{x})^\top J(\mathbf{x}), \quad (38)$$

where $g_{\mu\nu}(\mathbf{x}) = \sum_{i=1}^D (\partial f_i / \partial x_\mu) (\partial f_i / \partial x_\nu)$. Geometrically, g captures how infinitesimal distances in input space map to distances in the representation space \mathbb{R}^D . By computing g , we gain insights into how the native space becomes warped in the embedding space (Fig. 5).

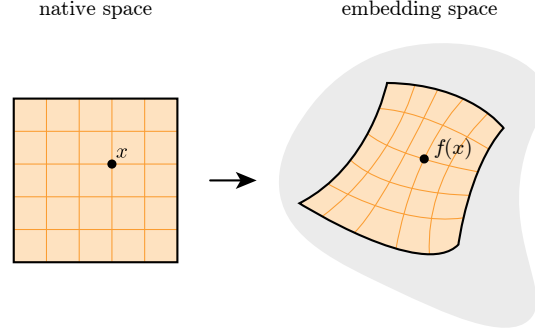


Figure 5. The action of the neural net can be imagined as wrapping of the (originally flat) native space (left) into the embedding space (right).

Volume Element. The local volume element is given by

$$dv(\mathbf{x}) = \sqrt{\det(g(\mathbf{x}))} dx_1 \dots dx_N. \quad (39)$$

This indicates how the network “stretches” or “distorts” volumes near each \mathbf{x} .

Factorization. While there is no single universal scalar for “factorization” in the N -dimensional case, one can investigate off-diagonal elements of $g_{\mu\nu}$ (or sub-blocks of the Jacobian) to see how strongly certain input dimensions (x_μ) mix with others (x_ν). For instance, if $\partial \mathbf{f} / \partial x_\mu$ is approximately orthogonal to $\partial \mathbf{f} / \partial x_\nu$ for all $\mu \neq \nu$, the representation preserves independence among coordinates.

B.2. Specialization to the 2D Case

When $N = 2$, let the input be (x, y) . Then the metric g is a 2×2 matrix:

$$g = \begin{bmatrix} \langle \frac{\partial \mathbf{f}}{\partial x}, \frac{\partial \mathbf{f}}{\partial x} \rangle & \langle \frac{\partial \mathbf{f}}{\partial x}, \frac{\partial \mathbf{f}}{\partial y} \rangle \\ \langle \frac{\partial \mathbf{f}}{\partial y}, \frac{\partial \mathbf{f}}{\partial x} \rangle & \langle \frac{\partial \mathbf{f}}{\partial y}, \frac{\partial \mathbf{f}}{\partial y} \rangle \end{bmatrix}. \quad (40)$$

Its volume element is

$$dv(x, y) = \sqrt{\det(g(x, y))} dx dy. \quad (41)$$

A Simple Factorization Metric in 2D. If one desires a single scalar capturing how “uncoupled” x and y remain, we can define:

$$\text{Factorization}(g(x, y)) = 1 - \frac{|g_{xy}(x, y)|}{|g_{xx}(x, y)| + |g_{yy}(x, y)|}, \quad (42)$$

where $g_{xx} \equiv g_{0,0}$, $g_{yy} \equiv g_{1,1}$, and $g_{xy} \equiv g_{0,1} = g_{1,0}$. In words:

- g_{xx} and g_{yy} measure how much the representation changes when moving purely in the x - or y -direction.
- g_{xy} captures cross-direction entanglement.
- The closer $\text{Factorization}(g)$ is to 1, the more orthogonal (uncoupled) these directions are in \mathbb{R}^D .

By averaging this score over a grid of (x, y) points, one obtains a global measure of whether the representation remains factorized or becomes entangled.

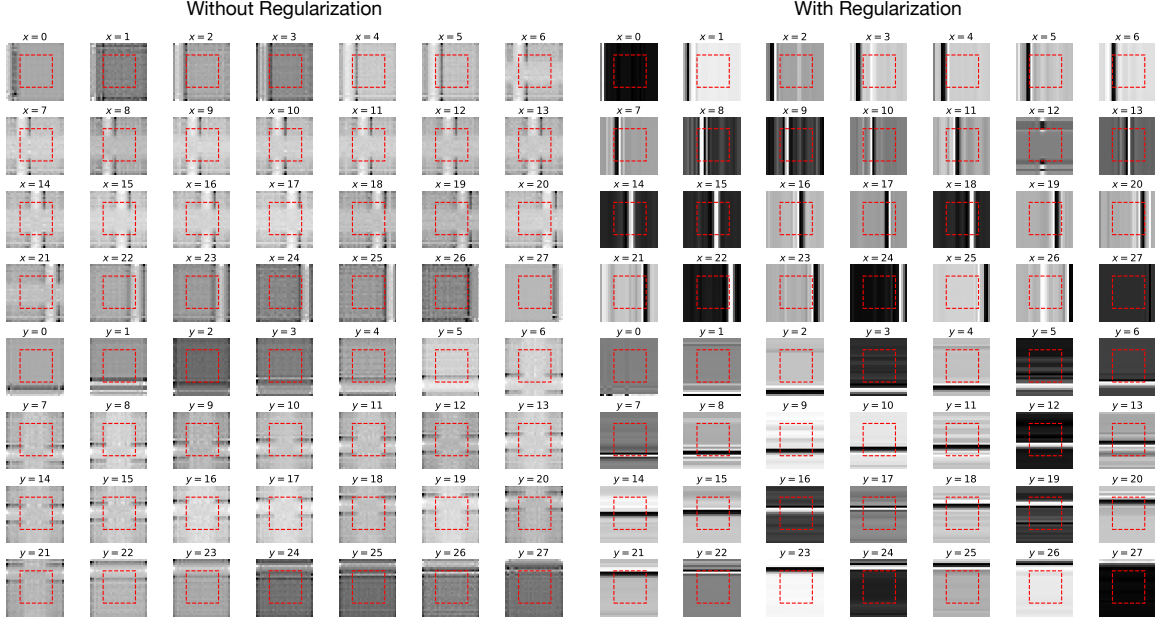


Figure 6. Visualization of x and y embedding matrices without and with regularization.

C. Low-rank Regularization for Compositional Generalization

In our generative approach, each input factor (e.g. the one-hot code for coordinate x or y) is mapped to a two-dimensional embedding matrix. Concretely, suppose we have a factor γ (which can be x or y), and we define a matrix

$$W_{i,j}(\gamma) \in \mathbb{R}^{d \times d}, \quad (43)$$

where the indices (i, j) correspond to a row and column in this 2D embedding. The matrix $W(\gamma)$ is then passed, possibly along with other embeddings, into subsequent layers (e.g. a small convolutional network) to produce the final output image.

Low-Rank Decomposition. To encourage each embedding matrix $W_{i,j}$ to remain factorized, we represent it via an SVD-like decomposition:

$$W_{i,j} = \sum_{n=1}^r v_i^{(n)} \lambda^{(n)} u_j^{(n)}, \quad (44)$$

where r is an upper bound on the rank, $\lambda^{(n)} \in \mathbb{R}$ are scalar coefficients, and $v_i^{(n)}, u_j^{(n)}$ are the row- and column-basis vectors for the n -th mode. We then regularize these parameters to encourage a low-rank and spatially consistent solution.

Entropy and Variance Penalties. First, we interpret the squared magnitudes $[\lambda^{(n)}]^2$ as a probability distribution across n ,

$$\tilde{\lambda}^{(n)} = \frac{[\lambda^{(n)}]^2}{\sum_{m=1}^r [\lambda^{(m)}]^2}, \quad (45)$$

and add an *entropy* penalty (DeMoss et al., 2024)

$$\mathcal{L}_{\text{ent}} = -\eta_1 \sum_{n=1}^r \tilde{\lambda}^{(n)} \ln[\tilde{\lambda}^{(n)}]. \quad (46)$$

Minimizing \mathcal{L}_{ent} reduces the distribution’s entropy, making only a few modes dominant (i.e. low rank).

Second, we penalize large row- or column-wise variance of the vectors $v^{(n)}, u^{(n)}$. Concretely, let $\text{Var}(v^{(n)})$ denote the sample variance of $v^{(n)}$ across indices i . Then we define

$$\mathcal{L}_{\text{var}} = \eta_2 \sum_{n=1}^r [\text{Var}(v^{(n)}) + \text{Var}(u^{(n)})]. \quad (47)$$

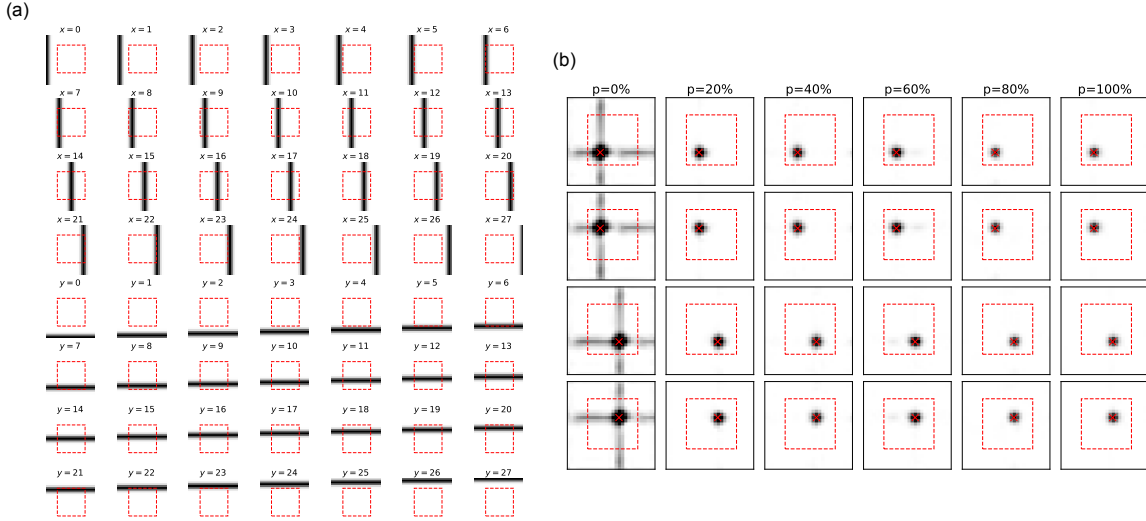


Figure 7. **Augmenting 2D Gaussian bump dataset with 1D Gaussian stripes enables compositional generalization.** (a) shows the 1D Gaussian stripe dataset for $N = 28$. (b) shows 4 sample generated OOD images for models trained on 1D Gaussian stripes + $p\%$ ID 2D Gaussian bumps subsampled.

Minimizing \mathcal{L}_{var} discourages the model from “memorizing” individual entries (i, j) , thus promoting spatial invariance. Summing both these terms along with the usual reconstruction loss (e.g. MSE) yields

$$\mathcal{L}_{\text{total}} = \mathcal{L}_{\text{MSE}} + \mathcal{L}_{\text{ent}} + \mathcal{L}_{\text{var}}. \quad (48)$$

By applying (44)–(46) to the embedding matrices for both x - and y -factors, the network learns a more factorized, compositional representation that generalizes better to unseen coordinate combinations. Fig. 6 demonstrate the 2D embedding matrices corresponding to different values of x and y in the cases *without* and *with* the entropy + variance regularization. In the case of no regularization, the model fails to preserve the integrity of the signal across the OOD region. In contrast, with regularization, each embedding matrix exhibits more pronounced vertical or horizontal banding that aligns cleanly with the chosen x - or y -coordinate. This indicates the network has discovered a more factorized structure, making it easier to recombine x and y to generate a 2D Gaussian bump in unseen OOD configurations.

D. Dataset Augmentation

One way of improving compositional generalization in our synthetic toy example is to *augment* the 2D Gaussian bump dataset with *1D Gaussian stripes*, thereby encouraging a more factorized representation in the pixel domain. Concretely, we generate *vertical* stripes by fixing a particular x -index and applying a 1D Gaussian along the y -axis, and *horizontal* stripes by fixing a y -index and applying a 1D Gaussian along the x -axis. Fig. 6(a) shows these stripes for $N = 28$, with each panel corresponding to a specific row or column coordinate. We then *combine* all stripes with a fraction $p\%$ of the original 2D bump dataset, so that examples of the 1D patterns are always present even when the 2D samples are subsampled.

This augmentation strategy allows the network to learn separate “axes” of variation (along x and y) more explicitly. Empirically, as shown in Fig. 6(b), models trained on these augmented datasets exhibit improved extrapolation to out-of-distribution (OOD) regions, even with limited 2D bump data. The presence of 1D stripes encourages a form of compositional inductive bias, wherein the model learns to *additively* combine horizontal and vertical factors in the pixel domain. Consequently, we gain the insight that guiding models toward simpler, factorized building blocks can significantly enhance their ability to recombine learned components in novel settings, an essential capability for robust compositional generalization.

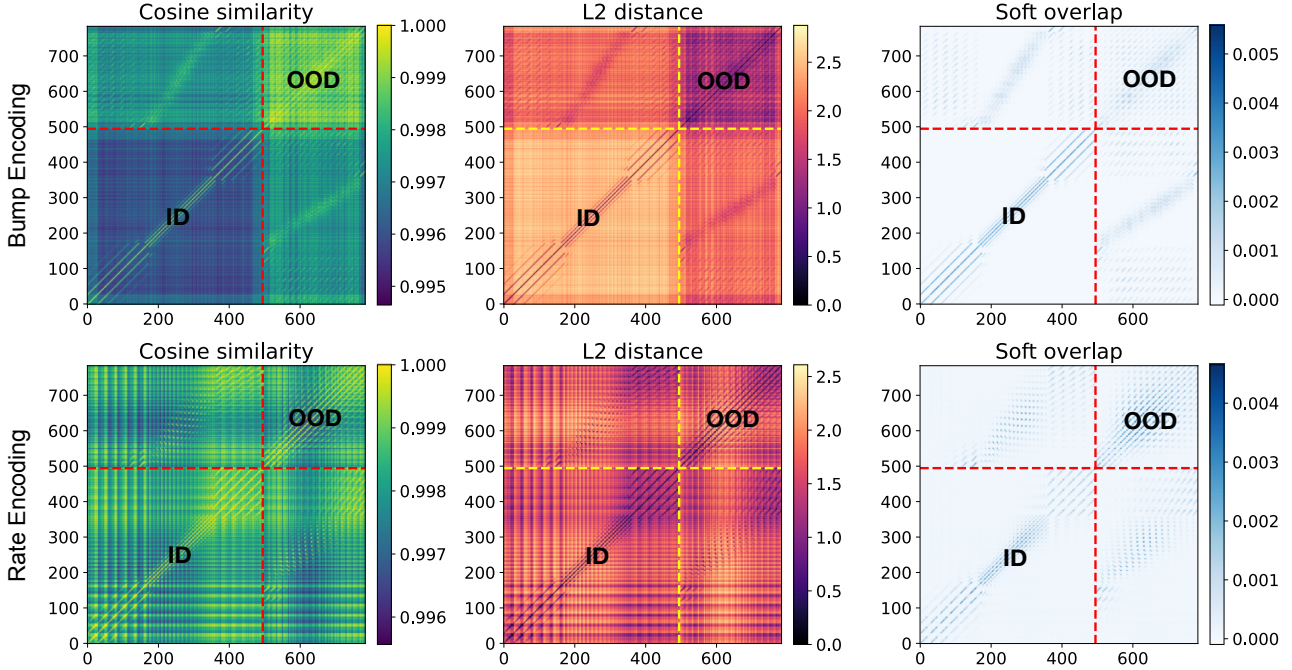


Figure 8. Full similarity/distance/overlap matrices visualization across the entire ID-OOD data distribution, compared between networks with bump (top) and rate (bottom) input encodings.

E. Supplementary Experimental Results

E.1. Full Kernel Characterization

In Sec. 3.3, we characterized the model’s OOD generalization behavior from a kernel-based perspective. In Fig. 1(e), we showed the agreement between the similarity (overlap) matrix with the theorized binary factorized kernel, which showed that the model independently “processes” novel input combinations of x and y . Here, we provide the full similarity/distance/overlap matrices across the entire generated dataset, ID and OOD. We note that Fig. 1(e) essentially shows a slice of what are shown in Fig. 8. We compare between generated image by models trained with bump-encoding and rate-encoding inputs, and the matrices are constructed based on three metrics: 1) cosine similarity, 2) L2 distance, and 3) pixel overlap. We notice that the kernel matrices of bump-encoded model exhibit stronger “block” structure as compared to those of the rate-encoded model. Here we note that the matrices have interesting diagonal structure from the non-finite width of the Gaussian bumps.

E.2. MNIST Digit Image Rotation Experiments

In Sec. 3.3, we mentioned that the phenomenon of activation superposition corresponding to memorized ID data seem to be generically applicable beyond the compositional setting. In Fig. 9, we present a simple toy experiment on rotating a single MNIST image data of number “4.” We generate a dataset of this rotated image “4” for various rotation angles $\theta \in [0, 360^\circ]$ while leaving out an OOD range $\theta^{\text{OOD}} \in (160^\circ, 200^\circ)$. We then train a CNN on the ID data, with input $(\cos \theta, \sin \theta)$, and test if the model can interpolate/extrapolate to the θ^{OOD} range. Unsurprisingly, the model fails to generalize to the unseen rotation angle range, as shown by the MSE plot in Fig. 9(a). Nevertheless, the generated OOD images reveal that the model performs linear interpolation between the edge-most ID samples, namely the images rotated at 160° and 200° . In Fig. 9(d), we show the linear interpolation between the ground truth rotated images at 160° and 200° , which strongly resembles the generated OOD images shown in Fig. 9(c). Intriguingly, in Fig. 9(b) we show that the UMAP-embedded latent representations across the network layers remain smooth without significant deformation, unlike the case of 2D Gaussian bump generation presented in the main text. Nonetheless, the OOD outputs of the model as linear interpolation of ID images confirms that the model is indeed memorizing all ID images and superposing the corresponding activation patterns, which

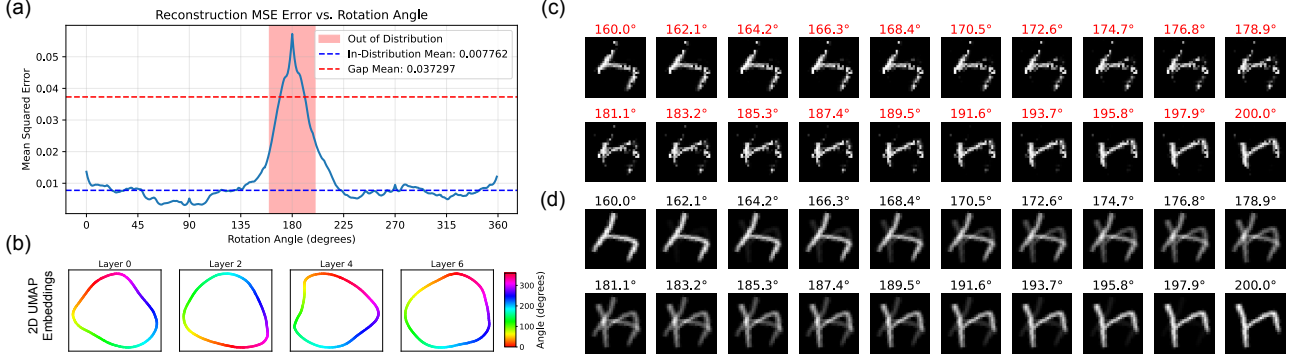


Figure 9. MNIST digit “4” image rotation experiment with OOD range of $160^\circ - 200^\circ$. (a) shows the reconstruction MSE as a function of rotation angle. (b) shows the 2D UMAP embeddings for representations at different layers of the network. (c) and (d) shows the generated rotated images in the OOD range vs. the pixel-wise interpolated images between 160° and 200° .

resonates with our findings for the 2D Gaussian bump generation experiment.

E.3. Volume Metric Plots and Generated OOD Images

In Sec. 3.4, we characterized manifold warping using the Jacobian based volume metric, as well as factorization and linear probe metrics as a function of layer depth. Here we show the same metrics for networks of different depths, for both CNNs (Fig. 11 and Fig. 12) and MLPs (Fig. 13 and Fig. 14). We also show the generated images as a function of network depth for CNNs in Fig. 10. An interesting phenomenon here is that the MLP models seems to have the opposite “warping” effect in the OOD region as compared to the CNN models. Moreover, the MLPs seem to have a smoother but more drastic degradation of factorization as a function of layer depth. Nonetheless, we expect similar conclusions regarding disentanglement and factorization to hold for CNNs and MLPs alike.

E.4. Neural Tuning Curves

In Sec. 4.2, we discussed the potential benefits of training models with augmented datasets that contain isolated factors of variation. Specifically, we showed that models trained with stripes+bumps are able to compositionally generalize in a data efficient manner. Mechanistically, the stripes provide the model a shortcut bias that leads the model to form additive composition in early layers of the network, which manifests as “stripe conjunctions,” which become “bumps” in downstream layers. In Fig. 15, we visualize four layers of a CNN trained with stripes only (left) and with stripes+100 bumps (right). Each sub-panel shows a 2D activation map for a selected neuron, along with its mean activation when collapsed over y (middle plot) or x (right plot). Across the layers, we observe that early-layer neurons primarily capture stripe-like features, with broader activations that vary more strongly along one dimension than the other. In deeper layers, these “stripes” begin to intersect more tightly, forming increasingly localized “bump”-like patterns. This indicates that the model is successfully learning to capture the complex compositional structures present in the augmented data, reflecting the additive-to-multiplicative transition in its internal representations. Furthermore, as bumps accumulate, the activations demonstrate a clear shift toward more focused and precise tuning, which supports the idea that the neural network is generalizing bump-like structures efficiently through additive composition early in the architecture and refining this understanding as the network deepens.

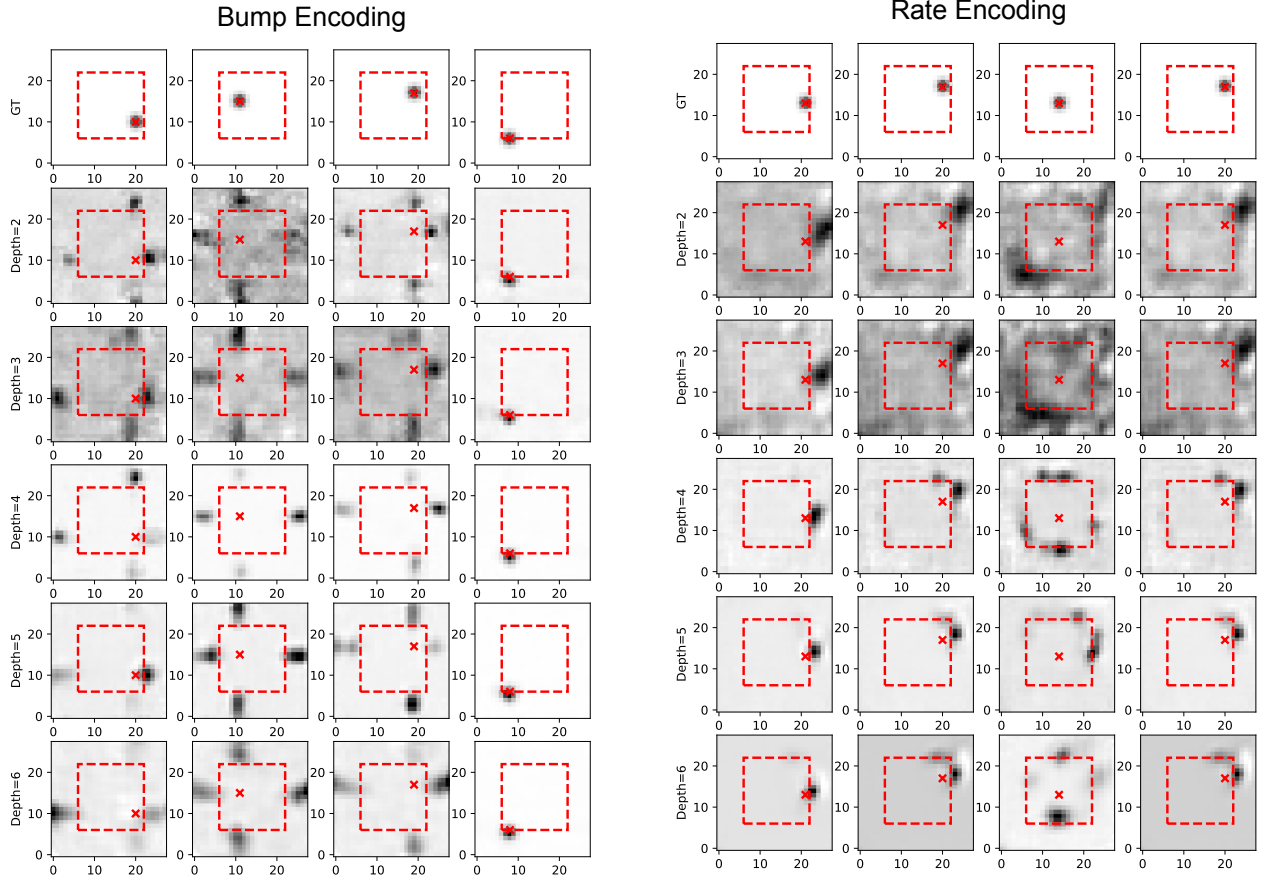


Figure 10. Comparison of generated OOD images for different network depths between networks with bump-based (left) and rate-based (right) input encodings.

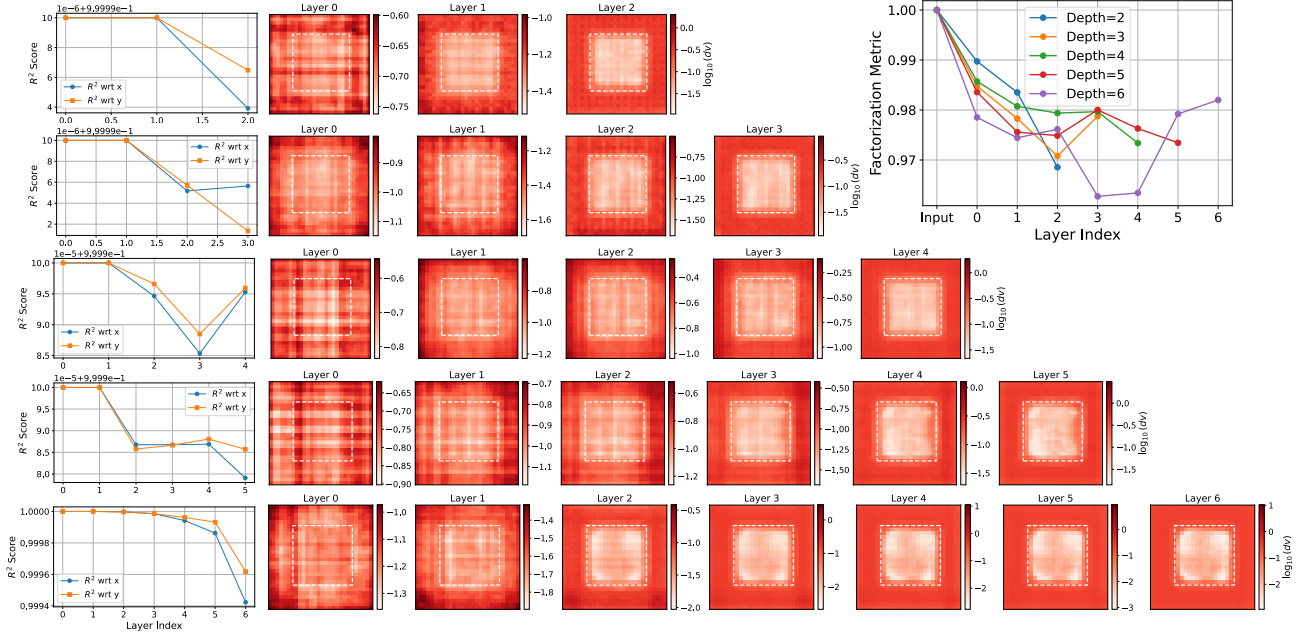


Figure 11. Evolution of manifold density and linear probe as a function of layer depth for different CNN network depths (bump encoding).

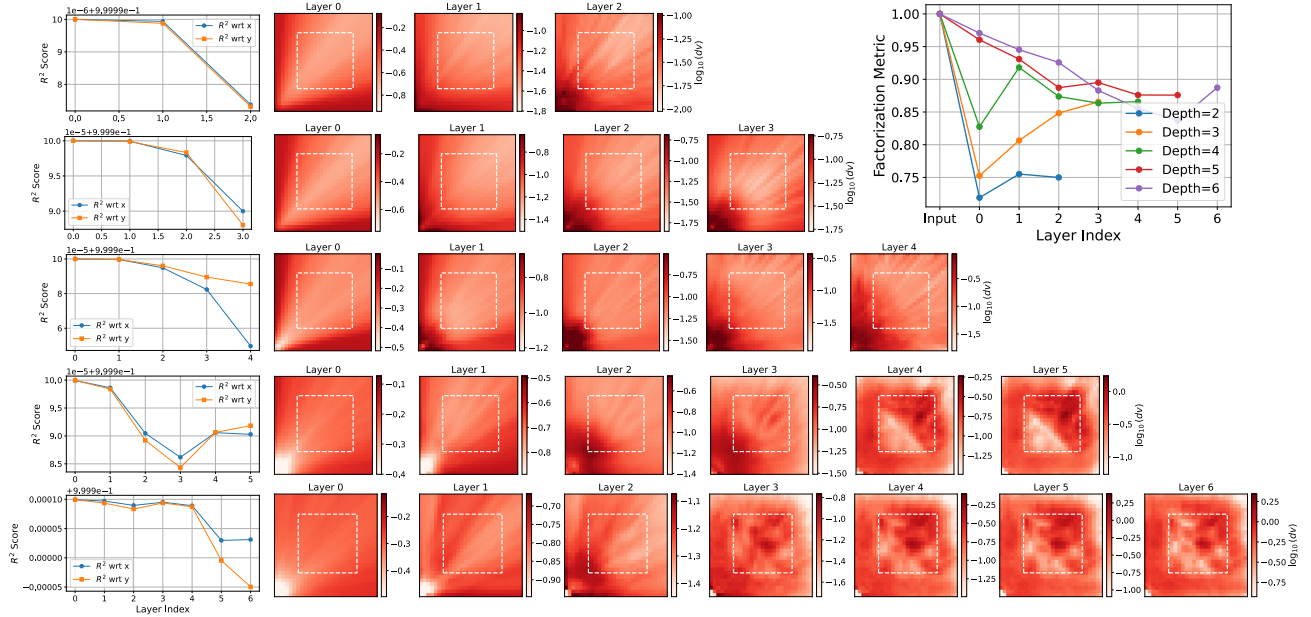


Figure 12. Evolution of manifold density and linear probe as a function of layer depth for different CNN network depths (rate encoding).

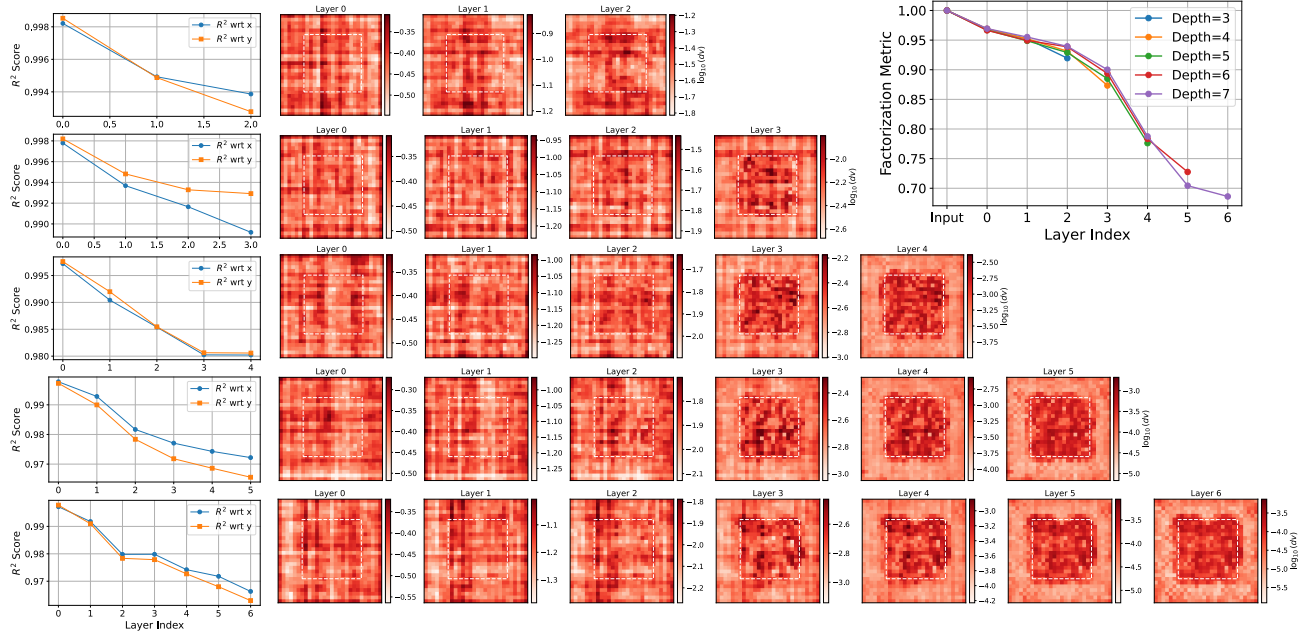


Figure 13. Evolution of manifold density and linear probe as a function of layer depth for different MLP network depths (bump encoding).

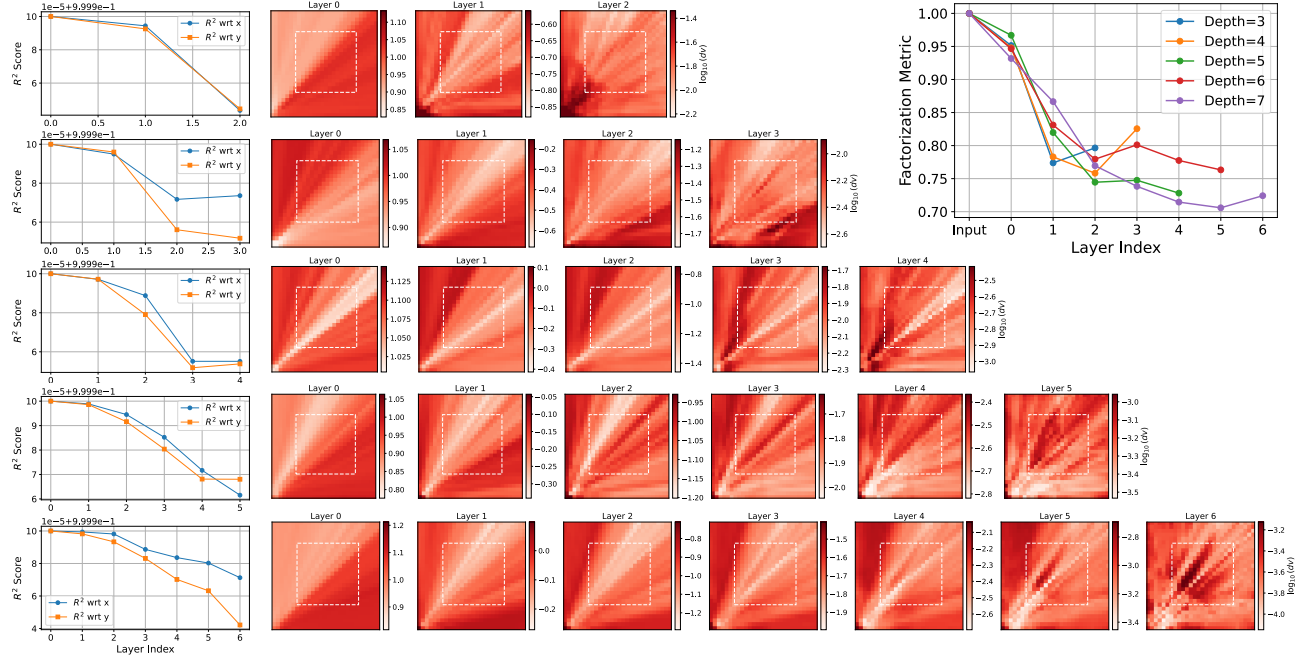


Figure 14. Evolution of manifold density and linear probe as a function of layer depth for different MLP network depths (bump encoding).

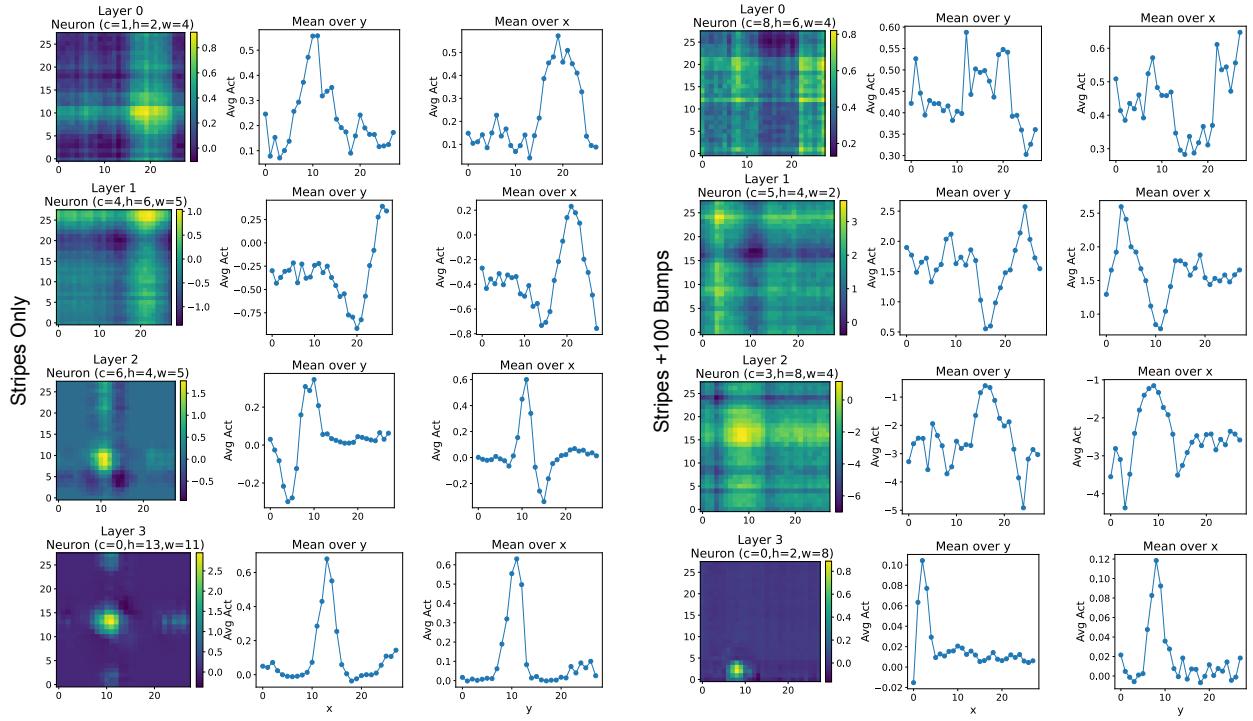


Figure 15. Neural tuning curves for sample neurons across different layers of a 4-layer CNN trained on a dataset of only stripes (left) and stripes + 100 bumps (right).